

See discussions, stats, and author profiles for this publication at: <https://www.researchgate.net/publication/322310594>

EnKF-Based Dynamic Estimation of Separated Flows with a Low-Order Vortex Model

Conference Paper · January 2018

DOI: 10.2514/6.2018-0811

CITATIONS

12

READS

451

5 authors, including:



Jeff D Eldredge
University of California, Los Angeles

161 PUBLICATIONS 3,770 CITATIONS

[SEE PROFILE](#)



Andre Fernando De Castro da Silva
Instituto Tecnológico de Aeronáutica

36 PUBLICATIONS 232 CITATIONS

[SEE PROFILE](#)



Tim Colonius
California Institute of Technology

581 PUBLICATIONS 21,333 CITATIONS

[SEE PROFILE](#)



David Williams
Illinois Institute of Technology

129 PUBLICATIONS 2,959 CITATIONS

[SEE PROFILE](#)

EnKF-based Dynamic Estimation of Separated Flows with a Low-Order Vortex Model

Darwin Darakananda*, Jeff D. Eldredge†

University of California, Los Angeles, Los Angeles, CA, 90095, USA

André Fernando de Castro da Silva‡ Tim Colonius§

California Institute of Technology, Pasadena CA 91125, USA

David R. Williams¶

Illinois Institute of Technology, Chicago IL 60616, USA

A data-driven vortex model of the unsteady aerodynamics of a two-dimensional separated flow is constructed. The vortex model relies on a standard collection of regularized vortex elements that interact mutually and with an infinitely-thin flat plate. In order to maintain a low-dimensional representation, with fewer than $O(100)$ degrees of freedom, a novel aggregation procedure is developed and utilized in which vortex elements are coalesced at each time step. A flow state vector, composed of vortex elements properties as well as the critical leading-edge suction parameter of Ramesh and Gopalarathnam (J. Fluid Mech., 2014), is advanced within an ensemble Kalman filter (EnKF) framework. In this framework, surface pressure measurements, sampled from a truth case, are used to correct the states of an ensemble of randomly-initiated vortex element models. The estimation algorithm is applied to several scenarios of a flat plate impulsively started at 20 degrees angle of attack at Reynolds number 500, in which the truth case comprises a high-fidelity Navier–Stokes simulation. The algorithm provides a good estimate of the flow as well as the aerodynamic force in both the baseline undisturbed case (a separated flow) as well as in the presence of one or more incident gusts, despite lack of a priori knowledge of the incident gust character.

I. Introduction

THE closed-loop control of the separated flow over an airfoil is essential for the development of highly agile aircraft whose flight is robust to atmospheric disturbances. These control strategies rely fundamentally on a low-order aerodynamics model that can accurately predict the force (and flow) response of an airfoil to arbitrary disturbances and/or actuation. Unfortunately, classical linearized quasi-steady and impulse response aerodynamic models have difficulty capturing the intrinsically non-linear force response that is observed when a separated flow is subjected to a broad spectrum of disturbances or actuation.¹ Thus, it is natural to consider phenomenological models that can capture this non-linearity in a direct—but inexpensive—manner. For this purpose, inviscid vortex models, in which advecting vortex elements represent the time-varying flow field through their mutually induced velocities, are a worthy candidate.

Inviscid vortex models have been in common use in recent years for predicting the dynamic response of a flow that tends to separate at the leading edge. One class of methods models the flux of vorticity into the wake by a routine release of constant-strength vortex elements from one or both edges of the airfoil.^{3,15,20} The models can be based on either discrete vortices (singular points or regularized ‘blobs’) or on vortex sheets, which, when numerically represented, are essentially discrete vortex elements whose interconnectivity has

*Graduate Student, MAE Dept., email: darwindarak@ucla.edu

†Professor, MAE Dept., email: eldredge@seas.ucla.edu. Associate Fellow AIAA.

‡Graduate Student, MCE Dept., email: andrefcs@caltech.edu.

§Professor, MCE Dept., email: colonius@caltech.edu. Associate Fellow AIAA

¶Professor, MMAE Dept., email: david.williams@iit.edu. Associate Fellow AIAA

been maintained. As the number of vortex elements increases, their interactions with each other result in the emergence of large-scale structures. These methods have been successful in modeling the detailed physics of the development of dynamic stall and the wake, but at the cost of tracking hundreds to thousands of vortices and their interactions.

To reduce computational cost, Wang and Eldredge¹⁸ modeled the large-scale structures using isolated point vortices with time-varying strength. The flux of vorticity into the fluid is then modeled by dynamically changing the strengths of these point vortices. While this second class of vortex model is much faster, it is unable to capture the natural formation of vortical structures that emerge from shear layer instabilities. Thus, Darakananda and Eldredge⁶ developed a hybrid representation in which the evolution of a vortex sheet rooted at each edge of a flat plate accounts for the natural roll-up of emerging vortex structures, and these structures are represented by variable-strength point vortices that siphon their strength from the end of each corresponding sheet. To ensure that this transfer does not spuriously affect the predicted aerodynamic force, an impulse matching principle, developed by Wang and Eldredge,¹⁸ was used to adjust the velocity of each variable-strength vortex.

A key open problem in vortex modeling is determining how much vorticity to release from the leading edge. While it is generally accepted that the Kutta condition is an acceptable vortex shedding criterion to use at the trailing edge, its use at the leading edge in numerous vortex models^{3,4,18} is mainly due to the lack of better criteria. This has driven the exploration of empirically-determined leading edge shedding criteria. In a discrete vortex model developed by Katz,¹³ leading edge shedding was tuned with a handful of parameters. Some parameters, such as the position of the leading edge separation point, were chosen based on experimental data, while others were adjusted to bring the predicted force closer to the measured force. In more recent work, Ramesh and Gopalarathnam^{14,15} introduced a shedding criterion based on the observation that real airfoils can support a modest level of suction around the leading edge before flow separation is triggered. Correspondingly, the authors suggested the use of the leading edge suction parameter (LESP), a measure of the integrated pressure at the nose of the airfoil, to govern vortex shedding. In their model, when the LESP is below a critical value, which we will denote as LESP_c , no vorticity is released. However, when the instantaneous LESP exceeds LESP_c , vortex elements will be released with the appropriate amount of strength to bring the LESP down to LESP_c . By tuning their discrete vortex model with an empirically determined LESP_c , the authors were able to predict lift responses that were in good agreement with experimental results. However, since the model was statically tuned, it has some difficulty handling real-time perturbations to the flow, such as gusts or other disturbances.

This lack of an obvious theoretical closure in the low-order model at the leading edge is a fortuitous consequence, for it opens the door to the development of data-driven vortex models, potentially suitable for real-time flow estimation. With this objective in mind, Hemati et al.¹¹ took another approach and posed the problem as one of constrained optimization, analogous to the underpinnings of optimal control theory. In this perspective, the leading and trailing edge vorticity fluxes were interpreted as inputs to a non-linear dynamical system. They then used variational methods to compute the time histories of these fluxes that would minimize the squared error between the empirically measured and model-predicted forces over some time horizon, subject to the constraint that the vortex elements move according to their usual dynamics. They applied this principle to optimize the variable-strength vortex model of Wang and Eldredge,¹⁸ using empirical force data from a high-fidelity simulation of the Navier–Stokes equations. While this optimization technique produced good results, it requires the measurements to be available over the entire optimization window. So while it is a useful post-processing tool, it is also not directly applicable for real-time estimation. In order to overcome this limitation, Darakananda and Eldredge⁸ developed a ‘bootstrapping’ procedure that applied the optimization over short time increments, accelerated by an initial guess obtained by regressing over previous time increments. However, in either form, this optimization framework relies on measurements of aerodynamic force from the ‘truth’ case. But these measurements are generally unavailable, and indeed, comprise part of the state that we seek to predict.

To address the shortcomings of previous approaches, in this paper, we approach the problem from the perspective of *data assimilation*, and investigate whether it is feasible to use real-time (and possibly noisy) sensor measurements to improve the prediction of a vortex model. To facilitate a more practical estimation strategy, we will only rely on surface pressure measurements, which will be folded into the predictive model through a Kalman filter (KF) framework. The Kalman filter consists of a predictive step, in which the state of the system is evolved with a dynamical model, followed by a measurement update, in which the state is corrected from new observations. Both the state’s mean and its covariance matrix—essential for determining

the degree to which measurements shall affect the state—are propagated in this framework. However, the requirements of tracking the covariance matrix render the algorithm intractably expensive for the moderate- or high-dimensional systems encountered in fluid flows. Thus, in this work, we will utilize an Ensemble Kalman Filter (EnKF), which was originally conceived to handle the high-dimensional non-linear dynamics found in meteorology.⁹ The EnKF obtains the covariance, as well as the mean state, from an ensemble of randomly-initiated instances of the state vector.

The EnKF has recently been investigated for its use in aerodynamics by da Silva and Colonius,⁷ in which the state prediction was obtained from a high-fidelity Navier–Stokes simulation. In the present work, the dynamical model comprising the state prediction in this framework will be a discrete vortex blob model. The state vector will be composed of the positions and strengths of all vortex elements, as well as—crucially—the value of the critical LESP. Thus, rather than assuming some prior knowledge of LESP_c , we will seek to estimate its value from the measured pressures. To ensure that the length of the state vector remains modest, we will aggregate the vortex elements by a novel identification procedure. The performance of this flow estimation framework will be assessed on undisturbed and disturbed separated flows past a flat plate, using high-fidelity numerical simulations as the truth from which pressure measurements are sampled.

II. Methodology

A. Aggregated vortex model formulation

The model used by Ramesh et al.¹⁴ is a standard vortex blob model, with a Kutta condition applied at the trailing edge, except that the leading edge vorticity flux is governed by the LESP criterion. We will utilize the same criterion here. The critical LESP provides a measure of the tolerance for leading-edge suction that does not lead to the flux of new vorticity into the fluid. It can also be interpreted as a critical angle of attack, below which the flow is deemed to be attached at the leading edge; a critical LESP equal to zero is equivalent to enforcing a Kutta condition at the leading edge. If the instantaneous LESP exceeds the critical value, then a vortex element is released from the edge, with strength proportional to the amount by which the critical LESP has been exceeded.

As an illustration of the role of critical LESP, in Fig. 1, we depict the vortex element distributions predicted by an LESP-based vortex blob model of a plate that is impulsively translated at 20° ; this will be the target problem of our studies in Section III. In the top plot, $\text{LESP}_c = 3.0$. This means that in order for the model to release any leading edge vorticity, we must have a large leading edge suction. Or equivalently, the model assumes that the plate can support a large amount of suction around the leading edge. The corresponding critical angle of attack is larger than 20 degrees, so no vorticity is ever released. In the middle plot, $\text{LESP}_c = 0.3$. Here, we see that the model predicts the formation of a coherent leading-edge vortex (LEV). Finally, in the lower plot of Fig. 1, where $\text{LESP}_c = 0.8$, we see the emergence of a weaker LEV.

In Fig. 2, we show the corresponding pressure distributions, where the top of each plot corresponds to the leading edge, the bottom corresponds to the trailing edge, and time increases in the x -direction. In the middle plot, we can clearly see the growth of a negative pressure region as it propagates along the plate chord. This corresponds to the development and evolution of a strong LEV. In contrast, we see from the top plot that there is no clear LEV, and the low pressure at the leading edge comes simply from the high LESP_c value. At the intermediate value of LESP_c , the LEV

Like most vortex models, the dimension of the system increases with every time step due to leading and trailing edge vortex shedding. The steady and unbounded increase of the state dimension prevents such models from being used in any real-time applications. This is essentially the same problem that the hybrid vortex sheet/point vortex model⁶ was constructed to solve. Unfortunately, while the hybrid model performed well for high angle of attack and pitchup problems, its use of vortex sheets makes it unsuitable for flows at low angles of attack. Instead, in this work we will rely on a discrete vortex blob model, similar to Ramesh et al.,¹⁴ but we will aggregate blobs at each step in order to maintain a modest population of vortex elements. Here, we will discuss the details of this novel aggregation scheme.

By using vortex blobs instead of vortex sheets, we lose the natural ordering of the vortex elements that was provided by the sheets. In the hybrid sheet/vortex model,⁶ the variable-strength point vortex associated with a sheet consumes its vortex sheet in sequence, starting from the sheet's wake end. For later description, let us label each of these consumed elements on the sheet as the ‘source’ and the variable-strength element as the ‘target’. In each time step, the strengths of successive source elements are transferred into the target until a threshold on error (the spurious change to the predicted aerodynamic force on the plate due to

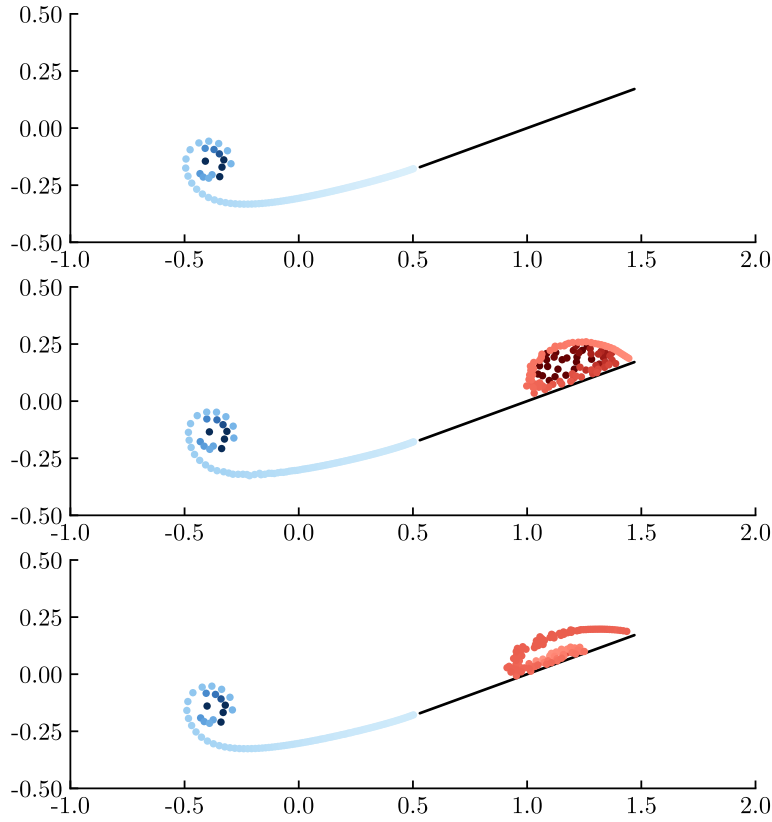


Figure 1. Comparison of vorticity distributions predicted by a vortex blob model after one convective time with different critical LESP values. (top): $\text{LESP}_c = 3.0$, (middle): $\text{LESP}_c = 0.3$, (bottom): $\text{LESP}_c = 0.8$

the transfer) is reached. When it becomes impossible to transfer any circulation from the sheet without exceeding the threshold, the target element turns into a classical constant-strength vortex and the tip of the vortex sheet is converted into a new variable-strength point vortex, i.e. a new target. The ordering in the sheet makes it always clear which vortex element consumes circulation and which one supplies it.

In contrast, in a vortex blob model, we lack an unambiguous relationship between vortex elements that can be exploited for aggregating these elements. Thus, in this work, we will take the most straightforward approach and simply test every possible combination of source-target pairs to determine which pairwise transfer will incur the least error in predicted force. We then perform the transfer on as many pairs as possible while keeping the accumulated error below a specified threshold, ϵ_F .

The vortex aggregation procedure is simply a modified version of the circulation transfer procedure described by Darakananda and Eldredge;⁶ as in that work, it requires that the velocity of the newly-aggregated vortex be modified to account for the flux of circulation from one vortex to another. Once we have set an appropriate value for ϵ_F , we do the following at every time step:

1. For every possible source-target pair of vortex blobs in the model, use Eqn. (17) in Darakananda and Eldredge⁶ to compute and store the hypothetical velocity correction to the target required if all of the source's circulation is transferred into the target.
2. Compute the (uncorrected) velocities of all vortex blobs and evolve the system forward by one time step.
3. Compute the impulse for each vortex blob at this end of this step.
4. For every possible source-target pair of vortex blobs in the system, first determine, from the velocity correction computed in step 1, the hypothetical impulse that the target blob would have if it had absorbed all the circulation from the source blob. Subtract from this the actual impulse of the source

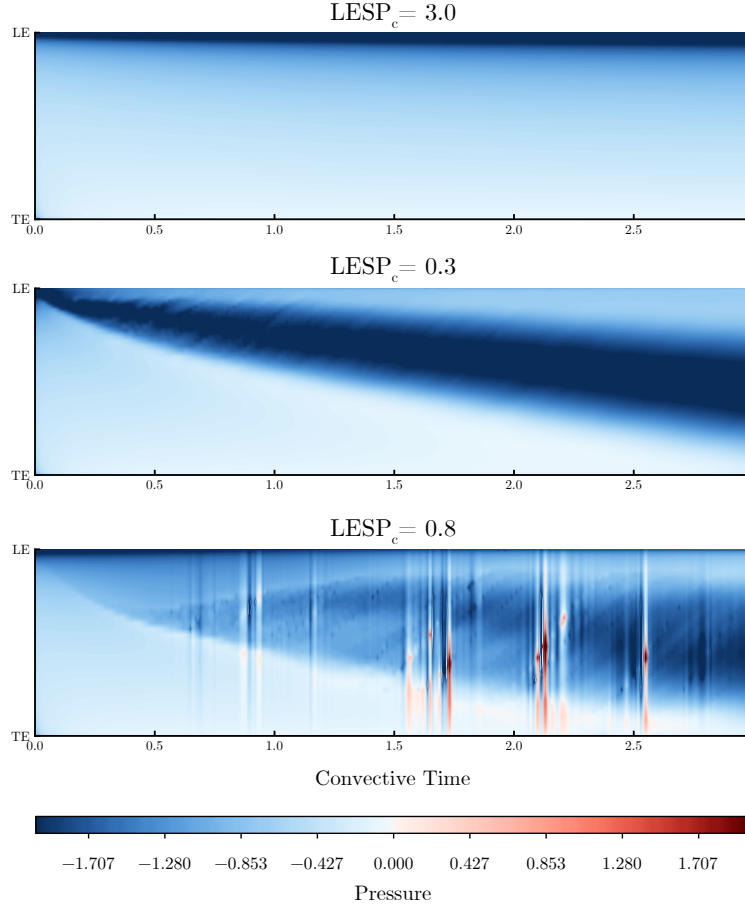


Figure 2. Comparison of pressure distributions across the plate predicted by a vortex blob model with different critical LESP values. (top): $\text{LESP}_c = 3.0$, (middle): $\text{LESP}_c = 0.3$, (bottom): $\text{LESP}_c = 0.8$

and target blobs, computed in step 3. This difference, when divided by time step size, is defined as the transfer error, and is a measure of the spurious force on the plate due to the aggregation.

5. Sort the source-target pairs based on the magnitude of their transfer error.
6. Starting from the pair with the lowest error, transfer circulation between as many pairs of vortex blobs as possible, stopping just before the accumulated error exceeds ϵ_F .

Although the procedure listed above contains multiple steps, with pairwise interactions that are usually undesirable, it also serves to prune a significant number of vortex elements in the system. In practice, the computational savings of keeping the state's dimensionality small far outweighs the cost of executing this procedure at every time step.

B. Ensemble Kalman filter approach

In this section, we present our data-driven vortex model. In Fig. 2 we observed a qualitative relationship between the critical LESP value and the evolving pressure distribution on the surface of the plate. This suggests that there may be a way to estimate LESP_c if we are given the surface pressure information. Even more importantly, it may be possible to use surface pressure measurements to directly augment missing parameters in our model. We will use a Kalman filter framework in order to algorithmically achieve this use of pressure measurements, as we will describe below. The classical Kalman filter is derived for linear systems. For weakly non-linear systems, it is popular to use the extended Kalman filter (EKF),¹⁰ in which the non-linear operators are linearized about the current state. However, the linearization can lead to

unstable growth of the error covariance. While this can be solved by using higher-order derivatives, the number of terms in the higher-order Tayler expansion grows substantially, which can make the computation prohibitively expensive for real-time applications. For our work, we will be using the ensemble Kalman filter (EnKF). The EnKF was introduced by⁹ explicitly to address two key shortcomings in the EKF: the need for explicit Jacobians of the dynamical model and the measurement function, and the large computational cost for high-dimensional systems. We will describe it in more detail in the following section.

1. The Ensemble Kalman Filter

The EnKF is essentially a Monte Carlo version of the classical Kalman filter. Instead of describing the distribution of the system state using a mean and a covariance, as in the classical and extended forms of KF, we approximate the distribution using an ensemble of size N of randomly-initiated members, where the state of the i -th member at time step k is denoted by $\tilde{\mathbf{x}}_{i,k}$. Suppose we know the ensemble states at time-step $k - 1$, we can propagate each member of the ensemble forward in time

$$\tilde{\mathbf{x}}_{i,k}^- = \mathbf{f}(\tilde{\mathbf{x}}_{i,k-1}) \quad \text{for } i = 1, 2, \dots, N, \quad (1)$$

where the superscript “ $-$ ” indicates that no measurements have been incorporated yet. Note that there is no additive noise term as it is assumed that the randomness is naturally introduced by having an ensemble. We now approximate the pre-measurement mean and covariance of the state with their sample values

$$\hat{\mathbf{x}}_k^- := \frac{1}{N} \sum_{i=1}^N \tilde{\mathbf{x}}_{i,k}^- \quad (2)$$

and

$$\mathbf{P}_k^- := \frac{1}{N-1} \sum_{i=1}^N \left(\tilde{\mathbf{x}}_{i,k}^- - \hat{\mathbf{x}}_k^- \right) \left(\tilde{\mathbf{x}}_{i,k}^- - \hat{\mathbf{x}}_k^- \right)^T. \quad (3)$$

We can then substitute the sample covariance into the standard definition of the Kalman gain without further modification

$$\mathbf{K}_k = \mathbf{P}_k^- \mathbf{H}_k^T \left(\mathbf{V}_k + \mathbf{H}_k \mathbf{P}_k^- \mathbf{H}_k^T \right)^{-1}. \quad (4)$$

While all members of the ensemble share the same Kalman gain, they each have their own innovation. In the original Kalman filter, the ‘innovation’ is defined as

$$\mathbf{y}_k := \mathbf{z}_k - \mathbf{H}_k \hat{\mathbf{x}}_k^-. \quad (5)$$

In defining the innovation for each ensemble member, we can replace $\hat{\mathbf{x}}_k^-$ with $\tilde{\mathbf{x}}_{i,k}^-$. However, we cannot use the same measurement \mathbf{z}_k for all ensemble members, as Burgers et al.⁵ found that doing so in an ensemble no longer reflects the fact that \mathbf{z}_k is drawn from a random variable \mathbf{Z}_k and will introduce spurious correlations in the ensemble covariance. Instead, we must artificially introduce noise into the innovation of each member of the ensemble

$$\mathbf{y}_{i,k} := \mathbf{z}_k + \boldsymbol{\epsilon}_i - \mathbf{H}_k \tilde{\mathbf{x}}_{i,k}^- \quad \text{for } i = 1, 2, \dots, N, \quad (6)$$

where the $\boldsymbol{\epsilon}_i$'s are drawn from \mathbf{V}_k . The Kalman update step is then applied to each member of the ensemble

$$\tilde{\mathbf{x}}_{i,k} := \tilde{\mathbf{x}}_{i,k}^- + \mathbf{K}_k \left(\mathbf{z}_k + \boldsymbol{\epsilon}_i - \mathbf{H}_k \tilde{\mathbf{x}}_{i,k}^- \right) \quad \text{for } i = 1, 2, \dots, N. \quad (7)$$

Further details, including several practical aspects for computing the Kalman gain from the ensemble statistics, can be found in da Silva and Colonius⁷

2. Covariance Inflation

The EnKF, just like the original Kalman filter, works to minimize the covariance of the estimated state distribution. However, unlike the Kalman filter, the EnKF does not use any information about the process noise when computing the ensemble covariance. Whereas the pre-measurement covariance of the standard Kalman filter, \mathbf{P}_k^- , is bounded from below by the covariance of the state disturbances, \mathbf{W}_k , there is no lower bound to the pre-measurement ensemble covariance. If we assume a non-zero measurement covariance \mathbf{V}_k ,

and an ever-decreasing ensemble covariance \mathbf{P}_k^- , then the Kalman gain of the ensemble eventually becomes negligible, after which all measurements are ignored by the EnKF. Methods for handling this covariance collapse are called covariance inflation. In general, covariance inflation modifies the ensemble states after computing the sample mean but before computing the sample covariance. Each ensemble state is updated by

$$\tilde{\mathbf{x}}_{i,k}^- \leftarrow \hat{\mathbf{x}}_k^- + \beta (\tilde{\mathbf{x}}_{i,k}^- - \hat{\mathbf{x}}_k^-) + \boldsymbol{\alpha}_{i,k}, \quad (8)$$

where β is the multiplicative inflation factor shared among all ensemble members, and $\boldsymbol{\alpha}_{i,k}$ is the additive inflation factor drawn from a random distribution at each time-step and for each ensemble member.^{2,17,19} After this update, we recompute the ensemble mean and compute the ensemble covariance. Whitaker and Hammill¹⁹ found that multiplicative inflation tends to be better at countering the effects of sampling errors, while additive inflation tends to be better at accounting for modeling errors. Multiplicative inflation tends to be easier to tune as it only involves adjusting a single value. Adjusting additive inflation, in contrast, requires more understanding about the actual dynamics of the underlying system.

3. Applying the EnKF to a vortex model

The state of our vortex model consists of the positions and strengths of the n vortex blobs, as well as the current estimate of the critical LESP

$$\mathbf{x}_{k-1} := \begin{bmatrix} x_{k-1}^1 & y_{k-1}^1 & \Gamma_{k-1}^1 & \cdots & x_{k-1}^n & y_{k-1}^n & \Gamma_{k-1}^n & \text{LESP}_{k-1}^c \end{bmatrix}^T. \quad (9)$$

The nonlinear state transition function \mathbf{f}_k propagates the state at time step $k-1$ by

1. computing the bound vortex sheet strength on the plate using the vortex blob positions and strengths
2. computing the velocities of the vortex blobs
3. advecting the plate and the vortex blobs
4. applying the vortex aggregation algorithm, reducing the strength of any aggregated blobs to zero instead of completely removing the blob
5. releasing a new vortex blob from each edge of the plate with strengths based on the Kutta condition at the trailing edge and the current estimate of the critical LESP (similar to Ramesh et al.¹⁵).

Note that the dimensions of the state increase by six (three per new vortex blob) after every state propagation step. Once all members of the ensemble have been propagated, we look for any vortex blobs that have zero strength across *all* members of the ensemble (in terms of its position/index in the state vector) and eliminate them from the ensemble states. This element elimination process, in conjunction with the vortex aggregation algorithm, keeps the dimension of the state vector in check. We then apply covariance inflation to the new ensemble states, before computing the pre-measurement ensemble mean $\hat{\mathbf{x}}_k^-$ and ensemble covariance \mathbf{P}_k^- with Eqs. (2) and (3).

Our measurements consist of M pressure differences along the plate at every time-step k

$$\mathbf{z}_k := \begin{bmatrix} \Delta p_k^1 & \cdots & \Delta p_k^M \end{bmatrix}^T. \quad (10)$$

Let us denote the pressure distribution predicted by the i -th ensemble member at time-step k as

$$\mathbf{m}_{i,k} := \mathbf{h}_k (\tilde{\mathbf{x}}_{i,k}^-). \quad (11)$$

Then the innovation for each member of the ensemble is given by

$$\mathbf{y}_{i,k} = \mathbf{z}_k + \boldsymbol{\epsilon}_i - \mathbf{m}_{i,k}. \quad (12)$$

Since pressure is definitely not a linear function on vortex properties, we need to linearize \mathbf{h}_k in order to compute the ensemble Kalman gain. One simple way is to define an augmented state vector

$$\mathbf{X}_{i,k} := \begin{bmatrix} \tilde{\mathbf{x}}_{i,k}^- \\ \mathbf{m}_{i,k} \end{bmatrix} \quad (13)$$

which admits the linear measurement function

$$\mathbf{H}_k := \begin{bmatrix} \mathbf{0}^{(3n+1) \times (3n+1)} & \mathbf{I}^{M \times M} \end{bmatrix}. \quad (14)$$

Then, denoting the mean predicted pressure distribution as

$$\bar{\mathbf{m}}_k := \frac{1}{N} \sum_{i=1}^N \mathbf{m}_{i,k}, \quad (15)$$

the covariance of the predicted pressure distribution as

$$\mathbf{M}_k := \frac{1}{N-1} \sum_{i=1}^N (\mathbf{m}_{i,k} - \bar{\mathbf{m}}_k) (\mathbf{m}_{i,k} - \bar{\mathbf{m}}_k)^T \quad (16)$$

and the cross-covariance between the state and pressure with

$$\mathbf{C}_k := \frac{1}{N-1} \sum_{i=1}^N (\tilde{\mathbf{x}}_{i,k}^- - \hat{\mathbf{x}}_k) (\mathbf{m}_{i,k} - \bar{\mathbf{m}}_k)^T, \quad (17)$$

we find that the ensemble covariance of the augmented state can be written as

$$\mathbf{P}_k^a := \frac{1}{N-1} \sum_{i=1}^N \left(\begin{bmatrix} (\tilde{\mathbf{x}}_{i,k}^- - \hat{\mathbf{x}}_k) \\ (\mathbf{m}_{i,k} - \bar{\mathbf{m}}_k) \end{bmatrix} \begin{bmatrix} (\tilde{\mathbf{x}}_{i,k}^- - \hat{\mathbf{x}}_k)^T & (\mathbf{m}_{i,k} - \bar{\mathbf{m}}_k)^T \end{bmatrix} \right) \quad (18)$$

$$= \begin{bmatrix} \mathbf{P}_k^- & \mathbf{C}_k \\ \mathbf{C}_k^T & \mathbf{M}_k \end{bmatrix}. \quad (19)$$

The Kalman gain of the pressure-augmented system is then

$$\mathbf{K}_k^a = \mathbf{P}_k^a \mathbf{H}_k^T \left(\mathbf{V}_k + \mathbf{H}_k \mathbf{P}_k^a \mathbf{H}_k^T \right)^{-1} = \begin{bmatrix} \mathbf{C}_k (\mathbf{V}_k + \mathbf{M}_k)^{-1} \\ \mathbf{M}_k (\mathbf{V}_k + \mathbf{M}_k)^{-1} \end{bmatrix}. \quad (20)$$

Since only the first block in the Kalman gain matrix above corresponds to the actual states we are interested in, we can write the EnKF Kalman update step for our system as

$$\tilde{\mathbf{x}}_{i,k} = \tilde{\mathbf{x}}_{i,k}^- + \mathbf{C}_k (\mathbf{V}_k + \mathbf{M}_k)^{-1} \left(\mathbf{z}_k + \boldsymbol{\epsilon}_i - \mathbf{h}_k(\tilde{\mathbf{x}}_{i,k}^-) \right). \quad (21)$$

III. Results

We demonstrate this method on three test problems with increasing complexity. The first case is impulsive translation of a flat plate of chord length c at velocity U at 20° angle of attack. The second case starts off the same way as the first, then we apply an incident disturbance after 3 convective time units. The last case builds on the second case by adding yet another disturbance after 4 convective time units. For our measurements, we probe the pressure differences across the plate at $M = 50$ points, with a distribution given by

$$\frac{c}{2} \cos\left(\frac{m\pi}{M+1}\right) \quad \text{for } m = 1, 2, \dots, M. \quad (22)$$

The pressure measurements we use are obtained from high-fidelity numerical simulations¹⁶ of the flat plate at $\text{Re} = 500$.

We use an ensemble size of $N = 50$ and initialize each ensemble member with a starting value of critical LESP drawn from $\mathcal{N}(0.5, 0.2)$. We set the error tolerance of the vortex aggregation procedure to $\epsilon_F = 10^{-3}$. For time-marching of the vortex model, we use the forward-Euler scheme with a fixed time-step of $U\Delta t/c = 0.01$.

A. No Pulse Actuation

The pulse-free case serves as a baseline for us to confirm our understanding of how pressure, critical LESP and the vortex model interact with each other. Fig. 3 and Fig. 8 respectively show the pressure distribution and force predicted by the EnKF-assisted model. In Fig. 9 we show the ensemble mean of the critical LESP over time. Then in Fig. 4 we show the number of vortex elements used by the model over time. Note that since we add and remove the same number of vortex particles to every member of the ensemble, the particle count history in Fig. 4 applies to any member of the ensemble. We show how using covariance inflation affects the variance of the ensemble state in Figs. 5 to 7. Finally, in Figs. 10 to 13, we compare the vorticity distributions predicted by the EnKF using different covariance inflation schemes at different convective times.

The top plot in Fig. 3 shows the pressure distribution given by CFD. This is the pressure distribution that we are trying to match. Visually, we can immediately see the growth of a LEV, indicated by the expansion of a negative pressure region towards the trailing edge. As the LEV stretches across the whole chord at around three convective times, it starts to entrain opposite-signed vorticity and trigger the growth of a TEV, which shows up as a thin sliver of negative pressure between three and five convective times. At around five convective times, we see a small positive pressure region at the trailing edge, which along with the diminishing TEV pressure signature, suggest the shedding of the TEV. These events are also observed at the corresponding times in the top right plots of Figs. 10 to 13, which show the vorticity contours predicted by the CFD.

The second plot in Fig. 3 shows the pressure distribution predicted by the EnKF ensemble mean when no covariance inflation is applied. We see a much more aggressive growth of the LEV in terms of both strength and density. We also see evidence of co-rotating vortices in the crisscrossing wave-like structure in the pressure distribution. Unfortunately, this indicates that the EnKF is not having any corrective effect on the model. This is consistent with our previous discussion of covariance collapse. In Fig. 5, we see that the ensemble variance of the states drop to negligible values almost immediately after we start running the model. Without any inflation to counter the covariance collapse, the EnKF essentially ignores the CFD pressure data.

The third plot in Fig. 3 shows the EnKF-predicted pressure distribution when a 5% multiplicative inflation is used. Although we can still visibly observe the pressure signature of co-rotating vortex blobs, we see that the LEV structure is more diffuse compared to the case without inflation. Looking at Fig. 6, we see that after the initial covariance collapse, the multiplicative inflation is able to slowly increase the variance of the vortex positions and strengths. However, the variance in the critical LESP is so small that it is immune to multiplicative inflation. This means that the EnKF can no longer influence the leading edge vorticity flux. To assimilate the pressure data, the EnKF can only rely on modifying the vortex positions and strengths. As a result, we often observe “teleporting” vortex blobs in videos, though it is difficult to show here through static figures.

The final plot in Fig. 3 shows the pressure distribution predicted by the EnKF after we apply both multiplicative and additive inflation. After tuning the inflation parameters, we found a suitable set of values:

- 1% multiplicative inflation
- additive perturbation to the vortex positions drawn from $\mathcal{N}(0, 10^{-5}c)$
- additive perturbation to the vortex strengths drawn from $\mathcal{N}(0, 10^{-3}\frac{1}{\Delta t})$
- additive perturbations to the critical LESP drawn from $\mathcal{N}(0, 5 \times 10^{-5})$.

We can clearly see that the predicted pressure distribution closely matches the CFD pressure distribution. This is further validated in Fig. 8, where the model-predicted force coefficient was computed using the rate of change of impulse rather than integrating the surface pressures. While there is some noise in the predicted force, we see that it agrees well with the CFD results.

The covariance inflation parameters were tuned to coerce the EnKF into favoring the modification of the critical LESP over the vortex blob positions and strengths. This stems from our underlying assumption that the key process is still governed by inviscid vortex dynamics, and assimilating pressure data through the EnKF simply provides a closure model to determine vorticity flux. If we look at Fig. 9, we see that the estimated critical LESP values remain relatively constant in time. Note that this does *not* mean that

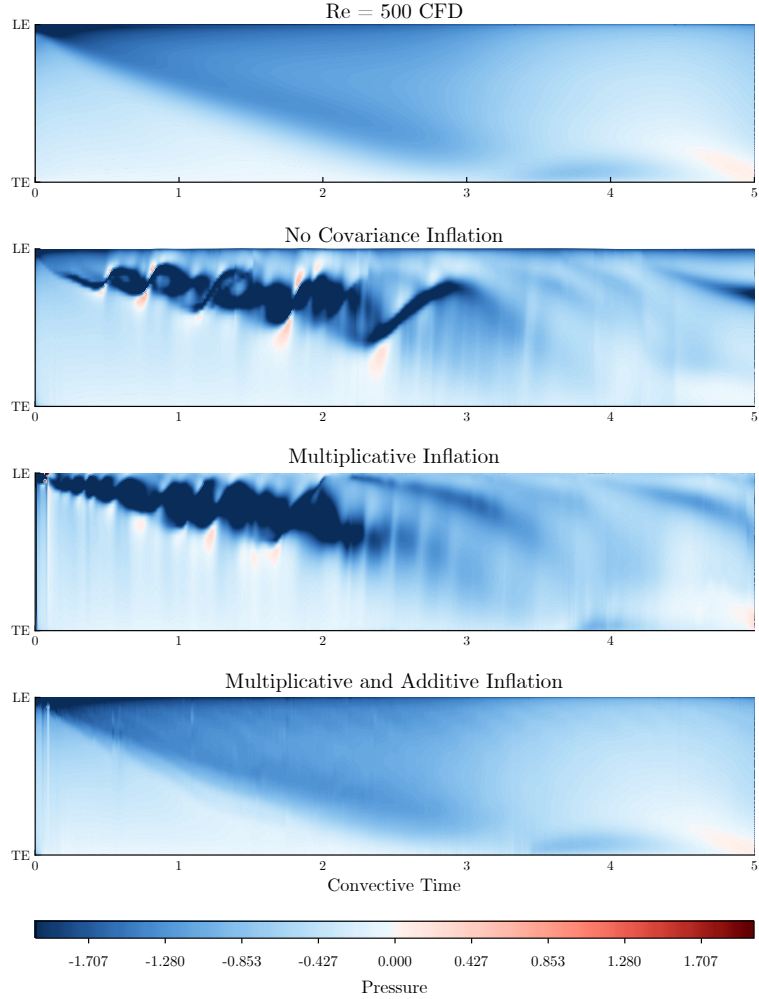


Figure 3. Comparison of the pressure coefficient distribution along the plate over time between the CFD results and EnKF predictions with various covariance inflation settings for the pulse-free case.

the leading edge vorticity flux is constant, since the vorticity flux required to maintain a fixed leading edge suction depends on the state of the ambient fluid. This result does seem to reflect the hypothesis from¹⁴ that the critical LESP value is mainly dependent on Reynolds number and relatively independent of the wing kinematics.

Comparing the placement of vortex blobs in Figs. 10 to 13, we see that the distributions predicted with both additive and multiplicative inflation are much more representative of the vorticity contours obtained from CFD. From Fig. 4, we see that even after five convective times, each member of the ensemble is only using about 40 vortex blobs. This tells us that the vortex aggregation procedure is also working correctly as it eliminated almost a thousand vortex particles without any adverse effects. With such a small number of vortex elements, it is surprising that the EnKF-assisted model was able to generate a LEV with such a diffuse pressure signature. Of course, as the EnKF can still make small changes to the vortex state, it may be worth investigating whether the EnKF is introducing some measure of viscosity into the model, via a random walk.

B. Single Pulse Actuation

Now we consider the case where a single incident pulse (a ‘gust’) is applied at the leading edge after around three convective time units. As with the pulse-free case, we start by considering the pressure distributions in Fig. 14. The top plot shows the pressure distribution predicted by high-fidelity CFD. We see that the initial

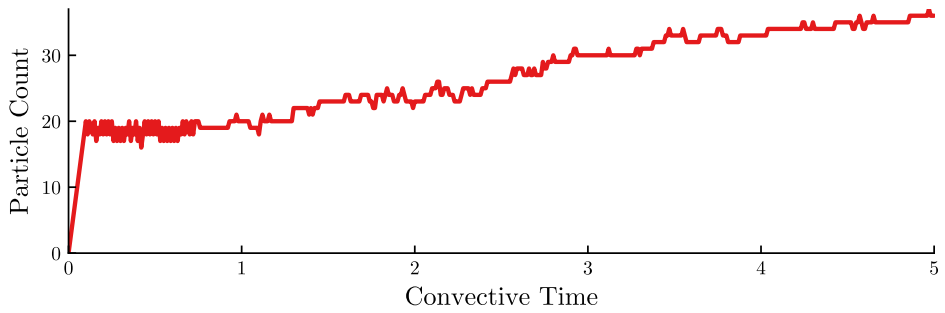


Figure 4. Number of vortex blobs used in the model over time when a combined multiplicative and additive covariance inflation is used for the pulse-free case

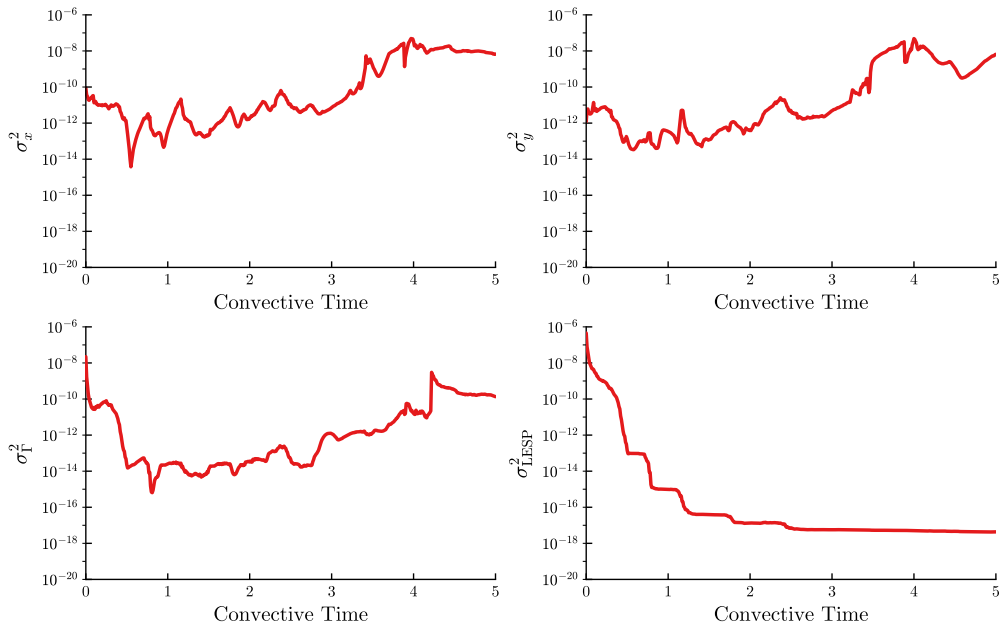


Figure 5. Ensemble variances for the pulse-free case without covariance inflation

development of the LEV is identical to the pulse-free case. At three convective times, we see the pulse as a band of negative pressure across the chord. Although the pulse itself is short-lived, we see that it triggers the growth of a new LEV. The new LEV is convected along the plate and into the wake, essentially returning the state back to the baseline separated state.

The second plot in Fig. 14 shows the pressure distribution predicted without covariance inflation. As expected, the covariance collapse makes the ensemble blind to the pulse. The appearance of the pulse on the pressure distribution predicted with multiplicative inflation, shown in the third plot of Fig. 14, indicates that the EnKF is attempting to assimilate the pressure data. At three convective times, we see that the predicted distribution of vortex blobs in the lower left plot of Fig. 20 still resembles the CFD vorticity contours on the figure's upper right plot. However, in Fig. 21, we see that while the CFD vorticity contours show the development of a new LEV, the EnKF with multiplicative inflation increased the strength of a vortex blob close to the trailing edge instead. Although it was able to push the predicted pressure distribution closer to the CFD results, the EnKF's heavy modification of the vortex states created very unnatural dynamics.

The EnKF-predicted pressure distribution that most closely resembles the CFD results came from using both additive and multiplicative inflation, shown in the bottom plot in Fig. 14. We use the same inflation parameters as the pulse-free case, which gives us a relatively stable set of ensemble variances, as shown in

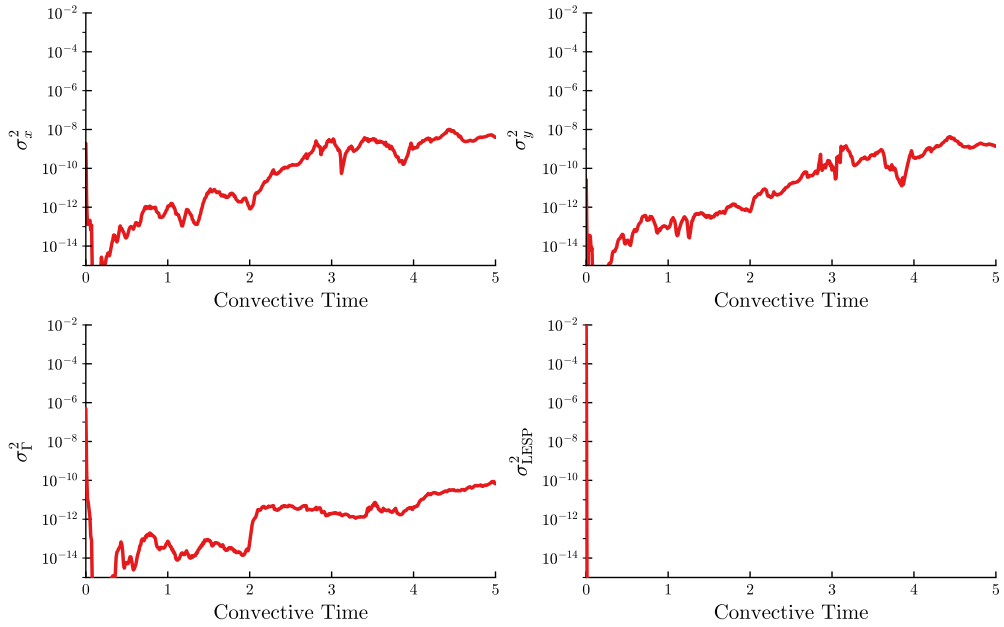


Figure 6. Ensemble variances for the pulse-free case with multiplicative covariance inflation

Fig. 18. Despite the fact that the sample variance in critical LESP is on the order of 10^{-8} , that amount of variation between the ensemble members is still enough that in Fig. 16, we see the EnKF responding to the measured pressure pulse by temporarily increasing the critical LESP. As the increase in critical LESP tends to reduce vorticity flux, we see that this small pulse in the critical LESP has the effect of severing the leading edge shear layer before developing a new LEV.

Comparing the distribution of vortex blobs in Figs. 20 to 23, we see that the corrections made by the EnKF seem to have the effect of spreading out the vorticity over a larger area. This is especially noticeable when comparing the results between the EnKF results with combined inflation (top left plots), and those without covariance inflation (bottom right plots). Even though the LEV was spread over more vortex blobs, we see in Fig. 17 that the vortex aggregation process has kept the total number of vortex particles very low.

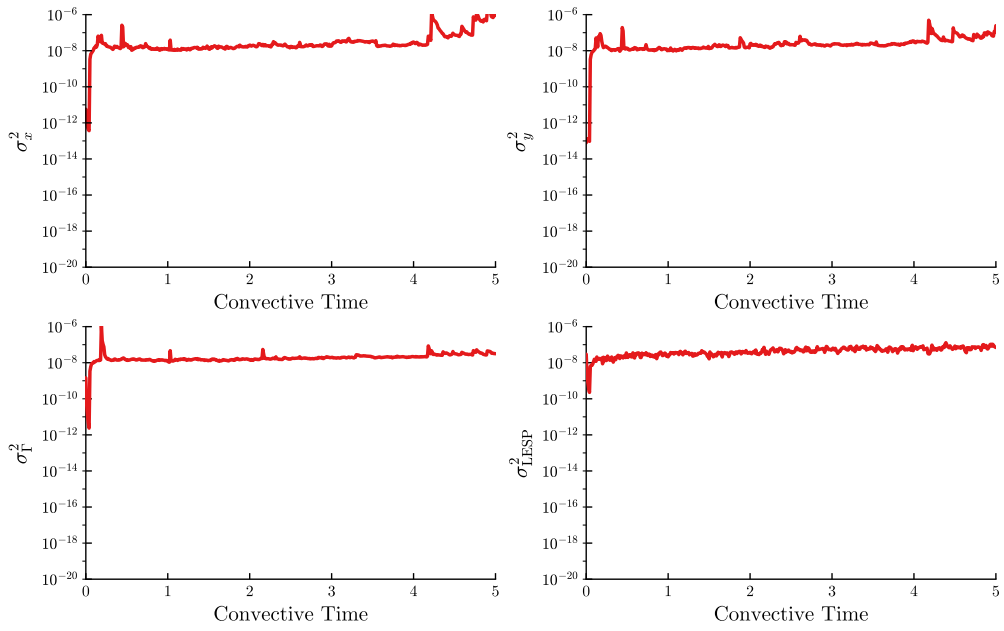


Figure 7. Ensemble variances for the pulse-free case with both multiplicative and additive covariance inflation

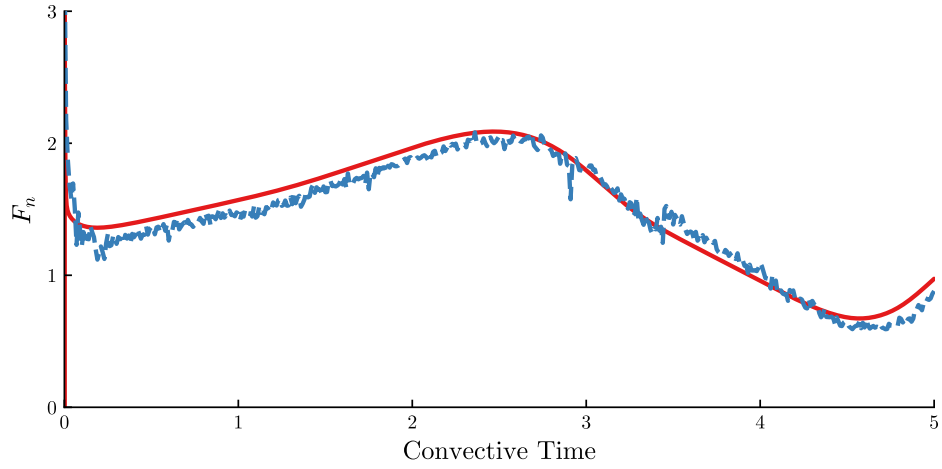


Figure 8. Comparison of the predicted normal force between (—) CFD results, and (—) EnKF ensemble mean for the pulse-free case.

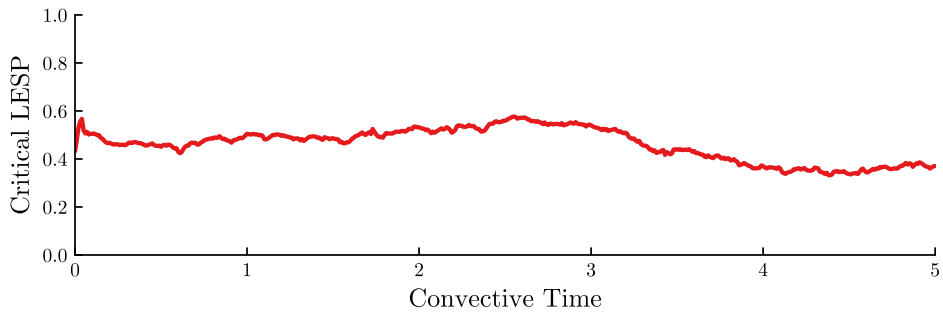


Figure 9. Time history of the ensemble mean value of the critical LESP for the pulse-free case

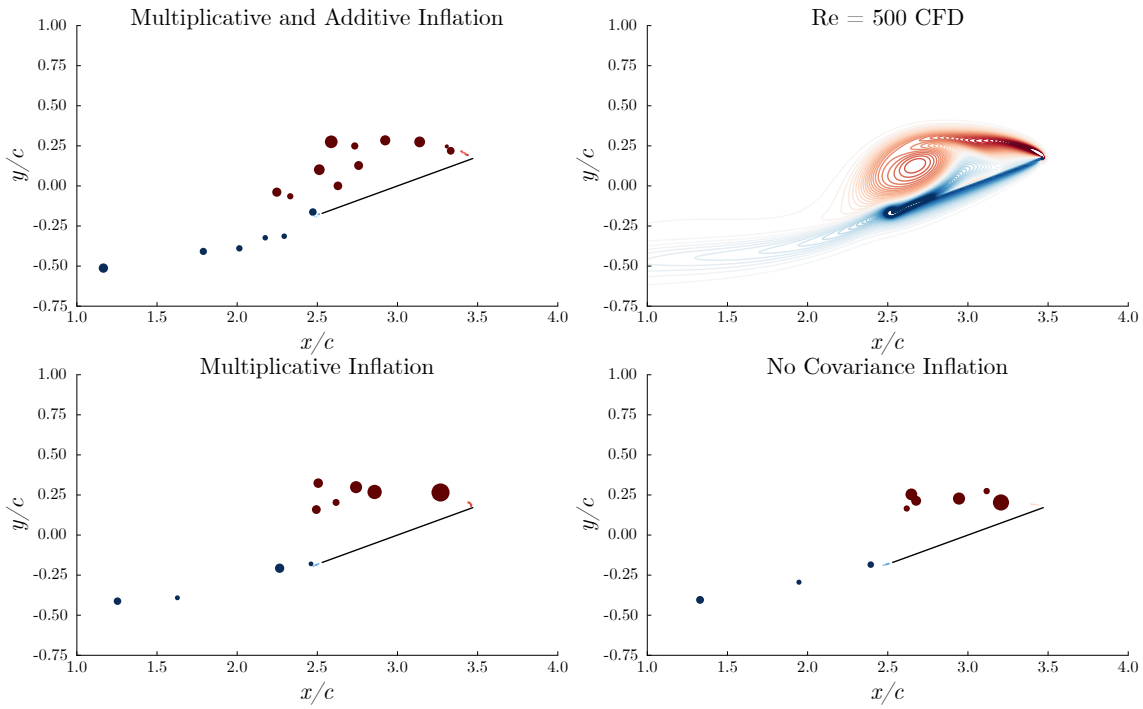


Figure 10. Comparison of the vorticity distribution for the pulse-free case at 3 convective times.

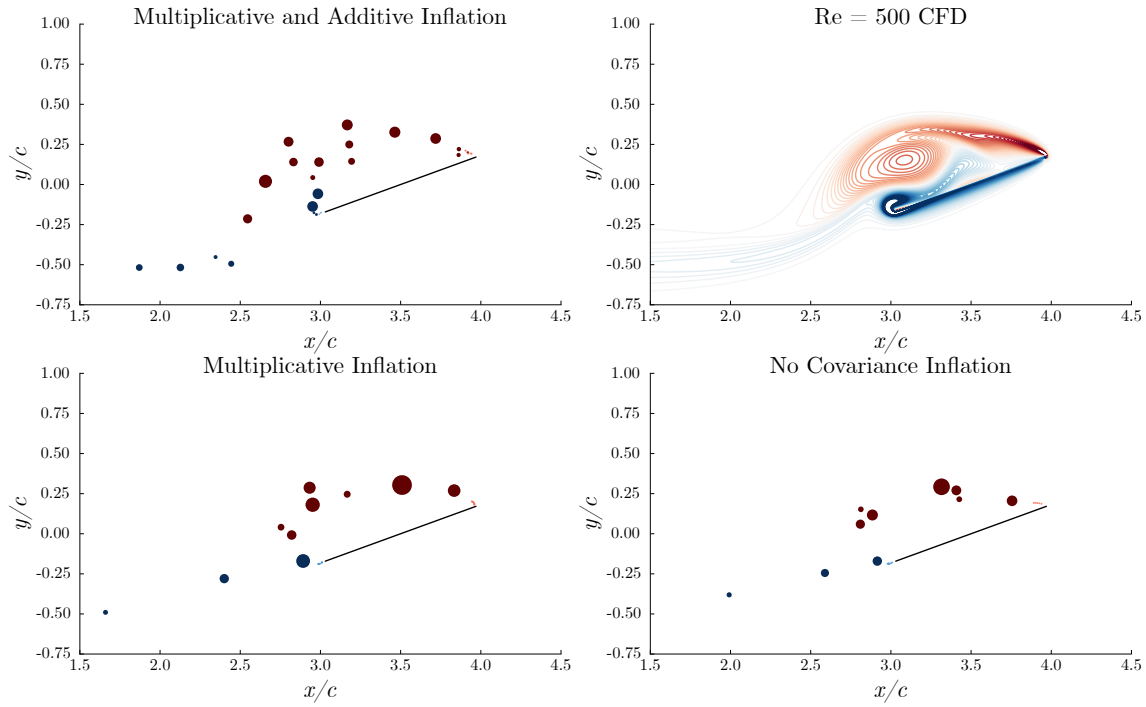


Figure 11. Comparison of the vorticity distribution for the pulse-free case at 3.5 convective times.

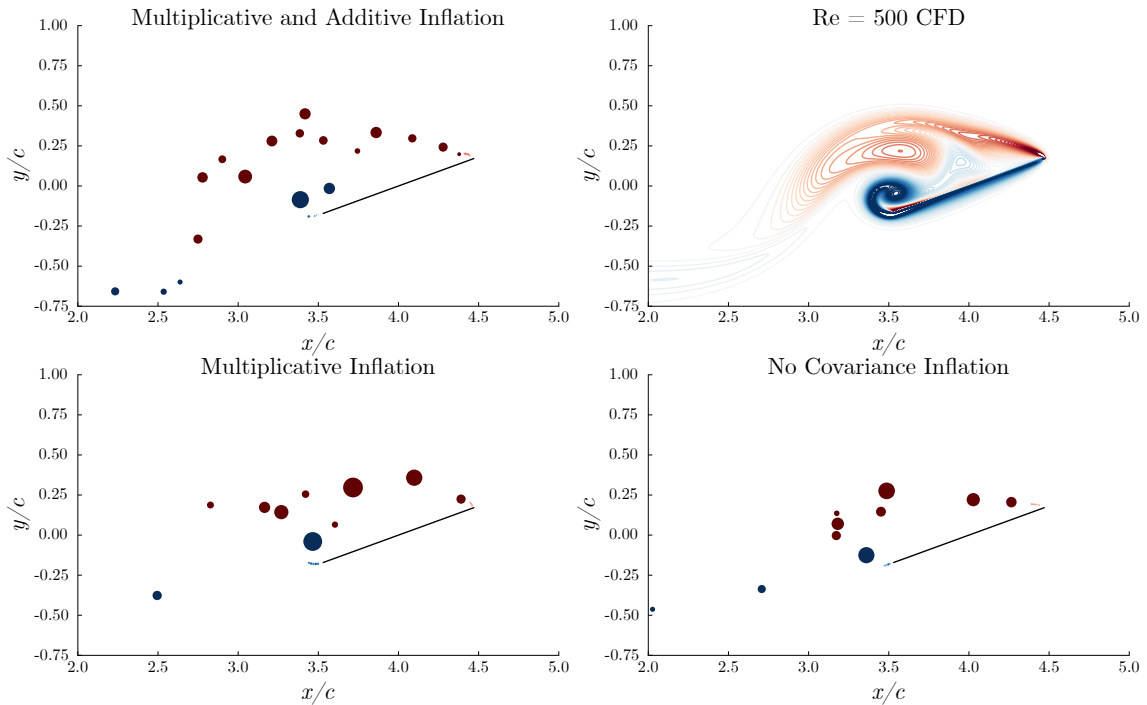


Figure 12. Comparison of the vorticity distribution for the pulse-free case at 4 convective times.

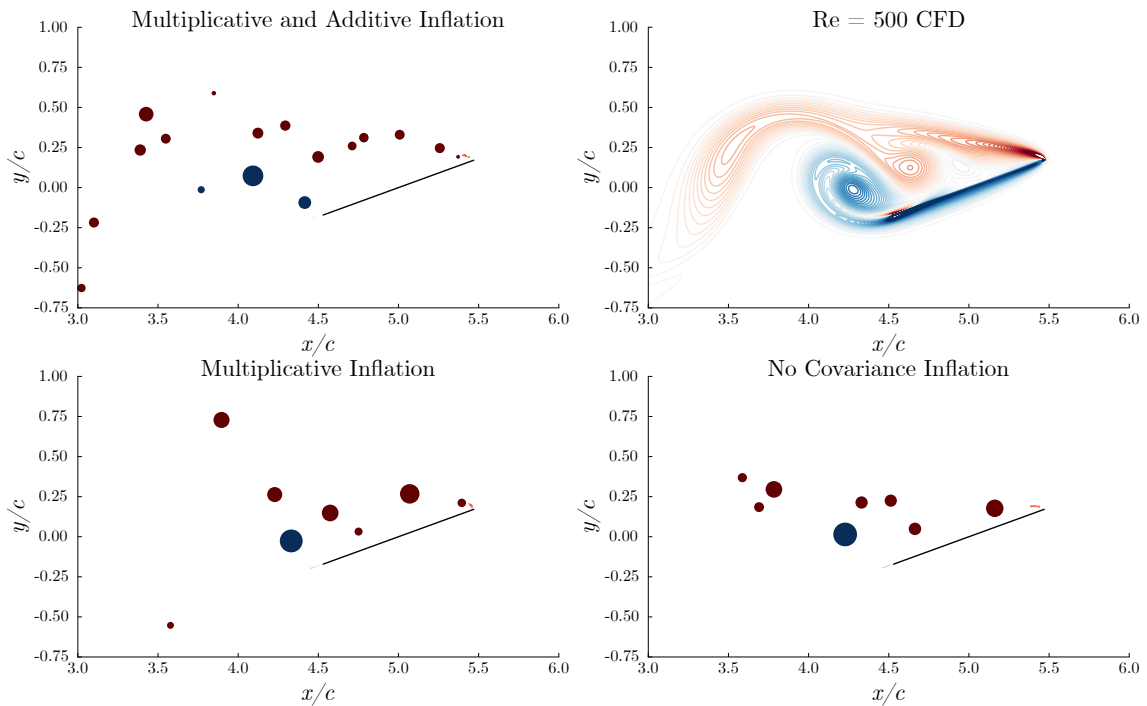


Figure 13. Comparison of the vorticity distribution for the pulse-free case at 5 convective times.

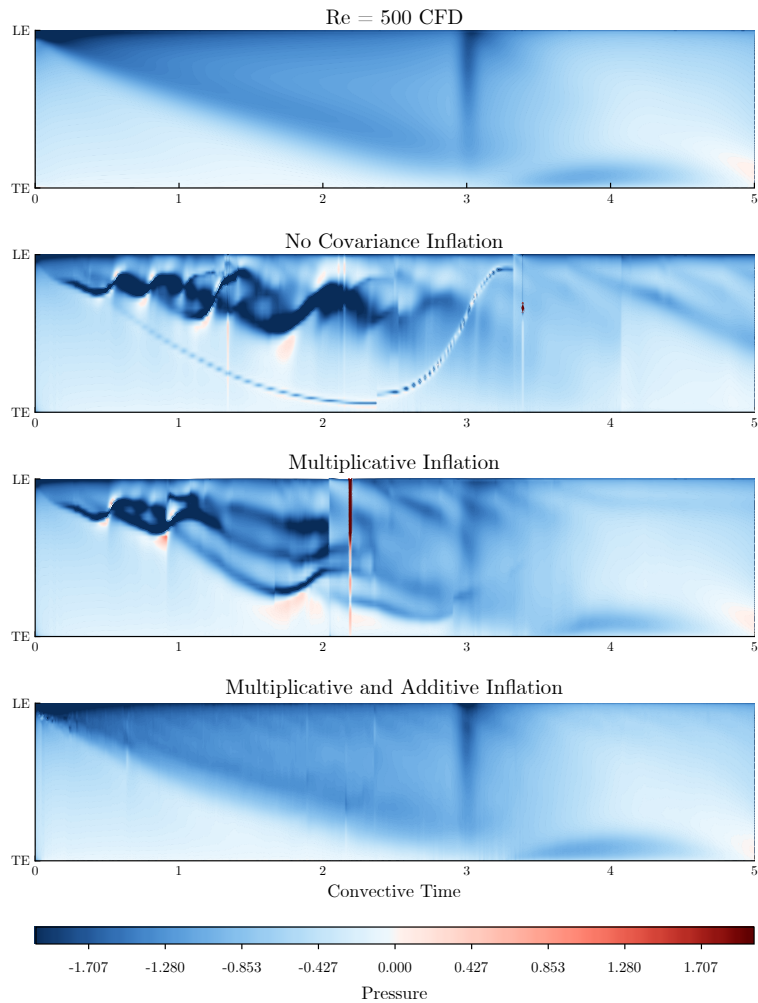


Figure 14. Comparison of the pressure coefficient distribution along the plate over time between the CFD results and EnKF predictions with various covariance inflation settings for the single pulse case

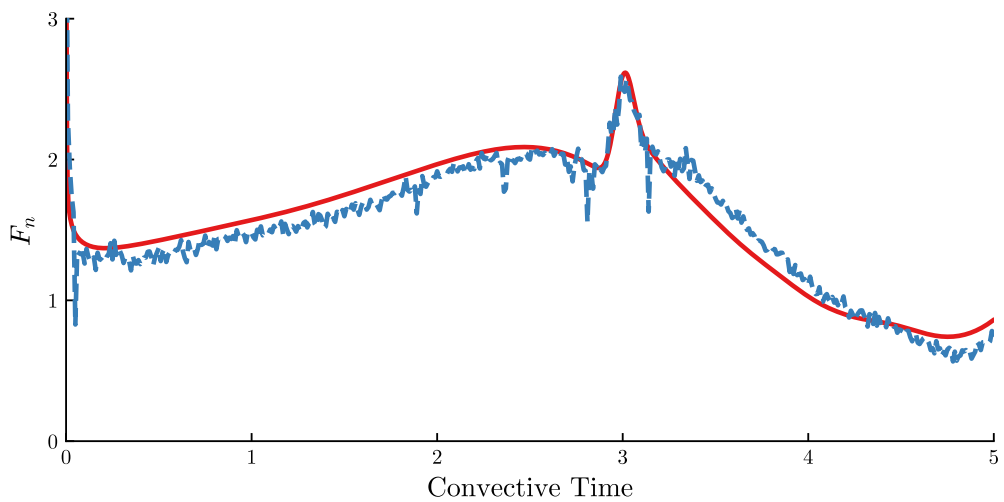


Figure 15. Comparison of the predicted normal force between (—) CFD results, and (---) EnKF ensemble mean for the single pulse case.

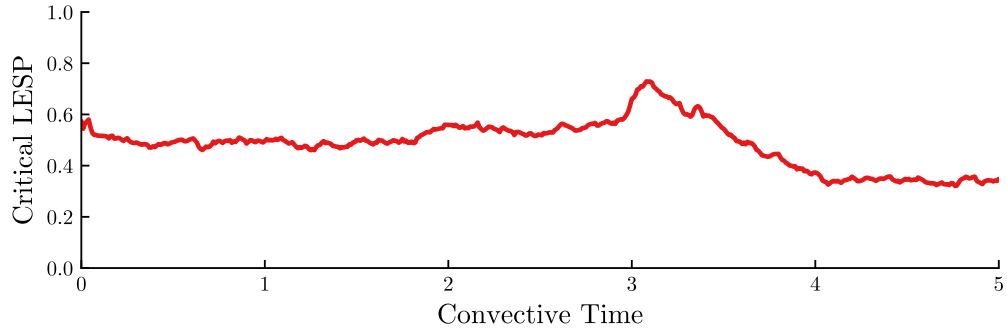


Figure 16. Time history of the ensemble mean value of the critical LESP for the single pulse case

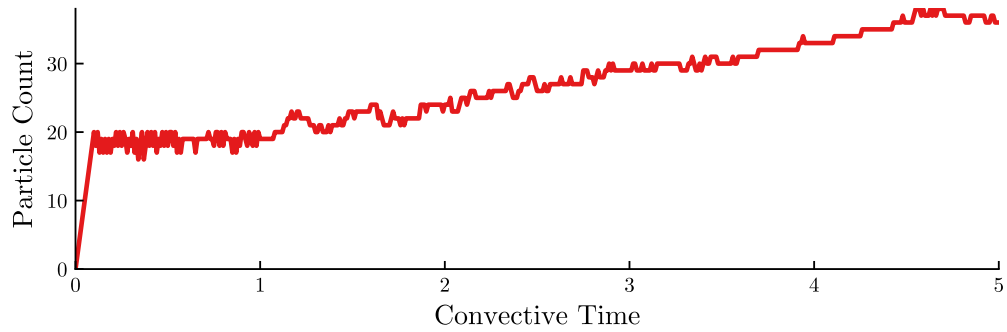


Figure 17. Number of vortex blobs used in the model over time when a combined multiplicative and additive covariance inflation is used for the single pulse case

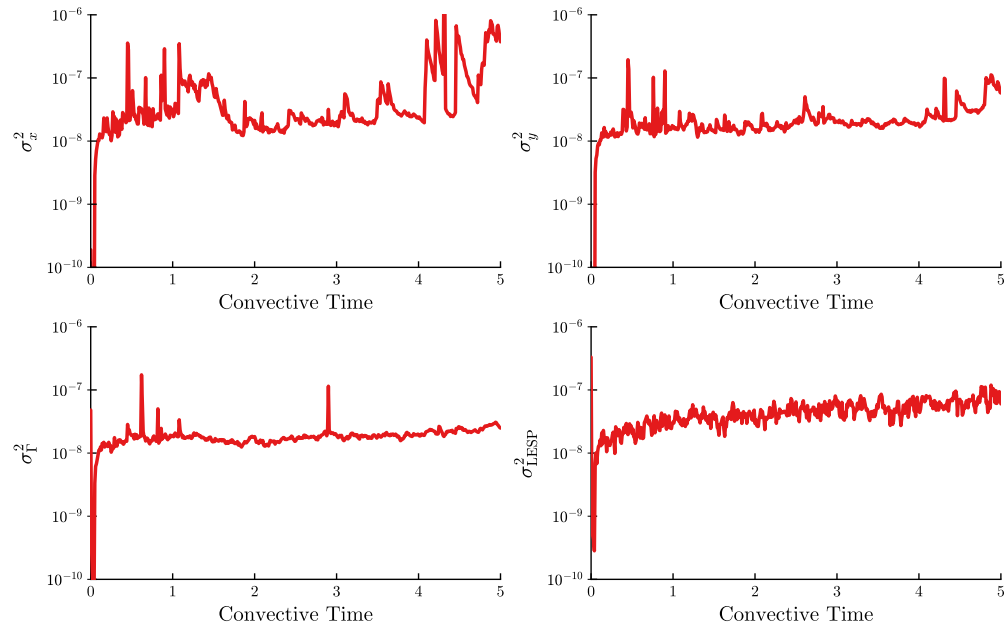


Figure 18. Ensemble variances for the single pulse case with both multiplicative and additive covariance inflation

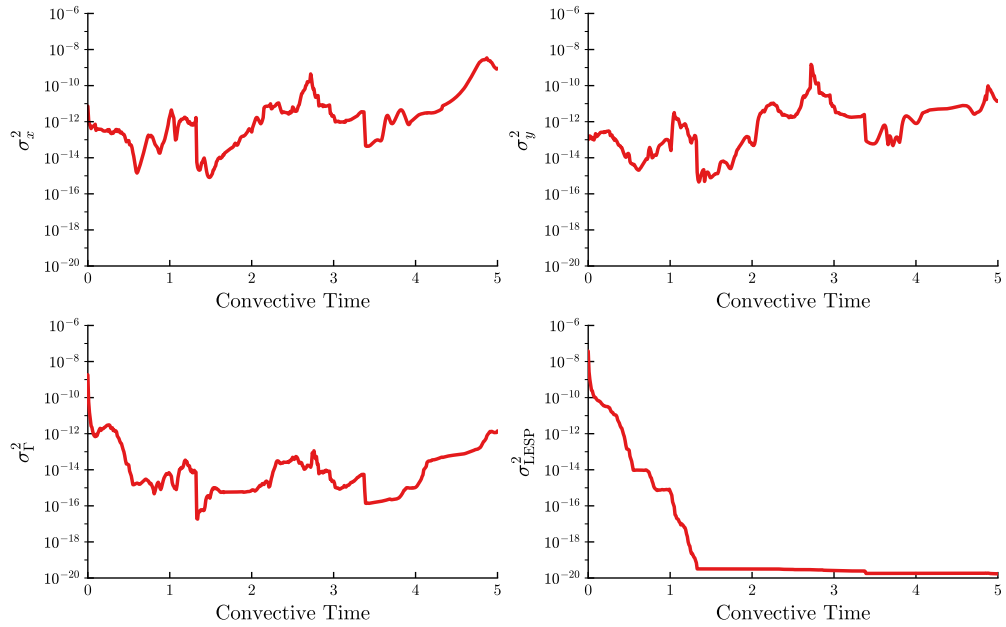


Figure 19. Ensemble variances for the single pulse case without covariance inflation

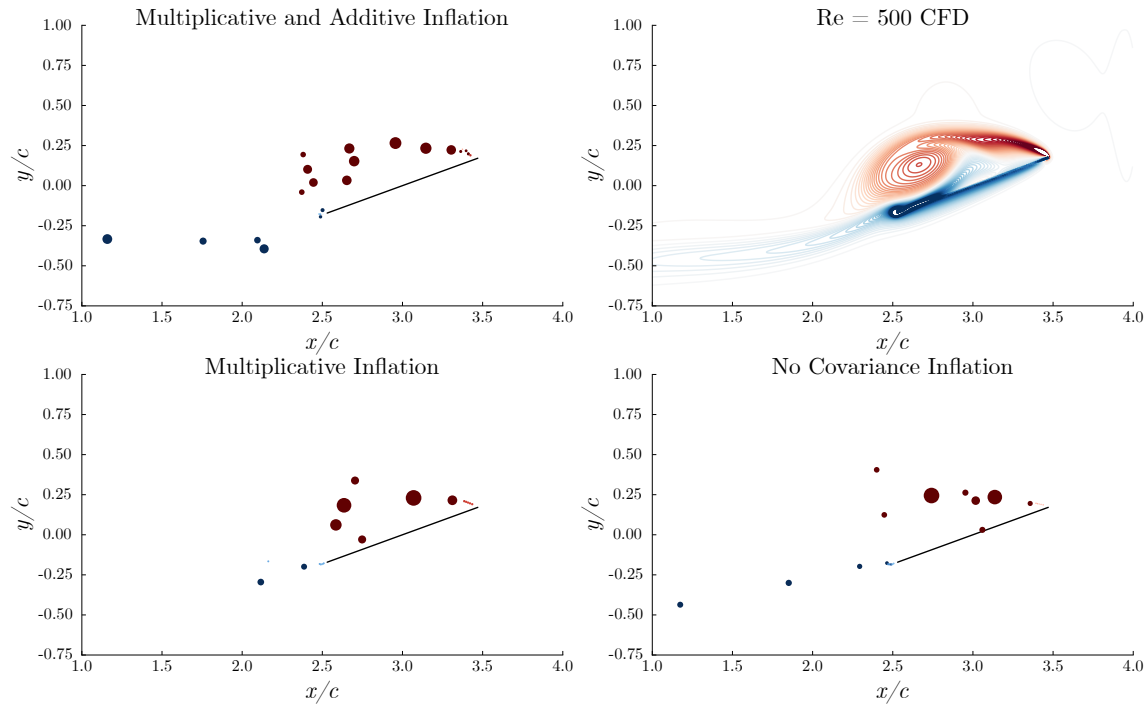


Figure 20. Comparison of the vorticity distribution for the single pulse case at 3 convective times.

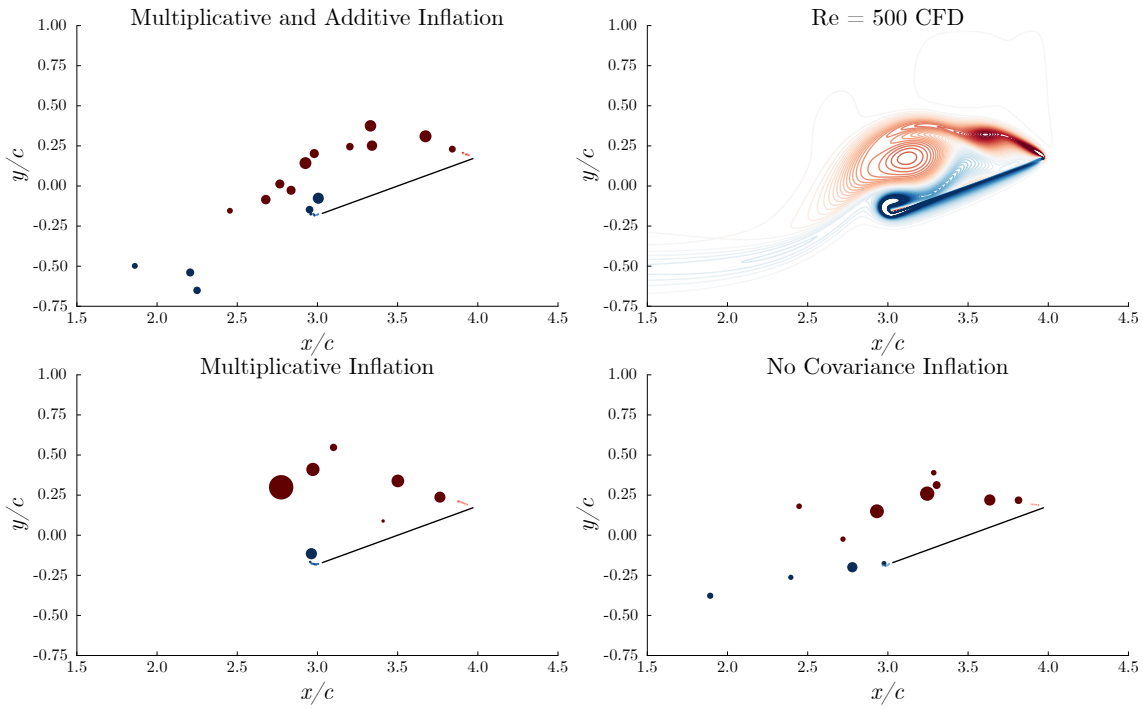


Figure 21. Comparison of the vorticity distribution for the single pulse case at 3.5 convective times.

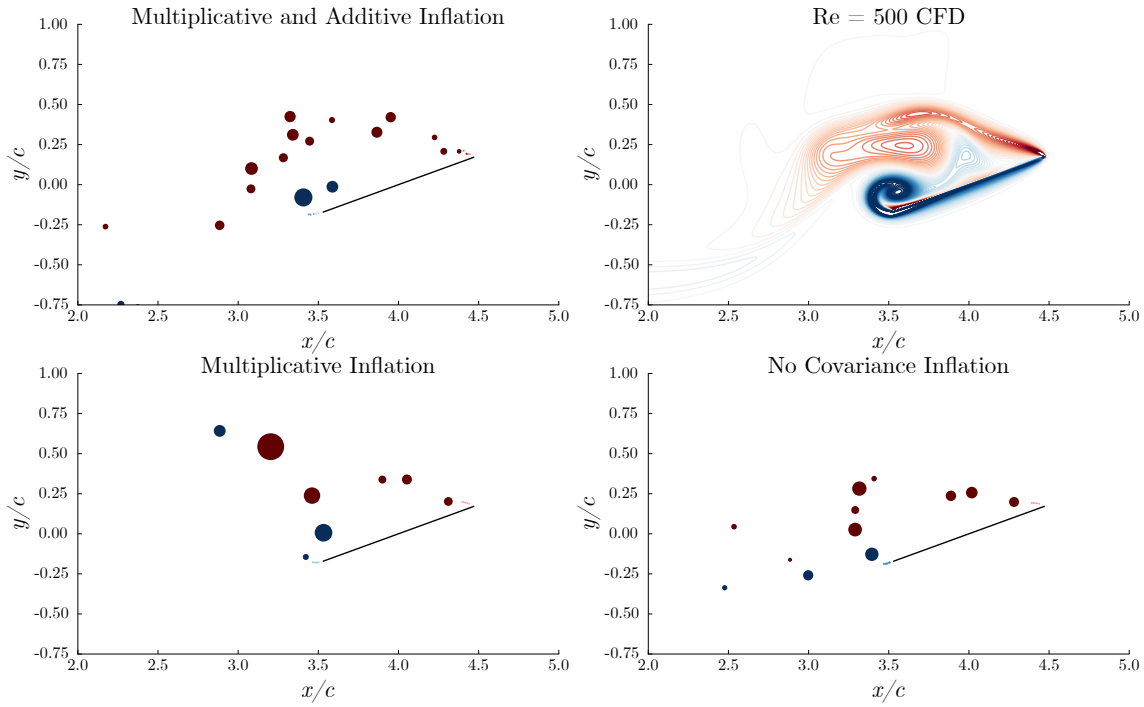


Figure 22. Comparison of the vorticity distribution for the single pulse case at 4 convective times.

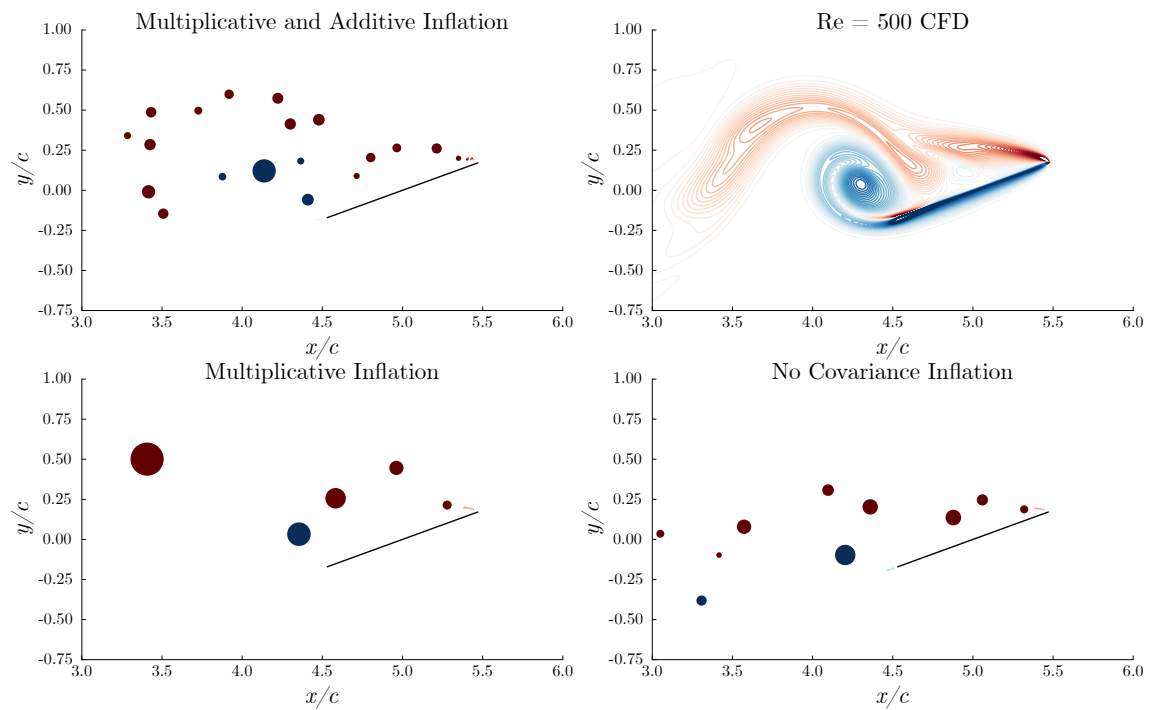


Figure 23. Comparison of the vorticity distribution for the single pulse case at 5 convective times.

C. Double Pulse Actuation

Finally, we look at the case with two incident pulses, one after three convective time units and another of the same strength after four convective time units. Since we also use the same covariance inflation parameters as the two previous cases, the results up to the second pulse are essentially the same as the results for the single pulse case, so we will just discuss the differences. From the pressure distribution in Fig. 24, force comparison in Fig. 25, and critical LESP history in Fig. 26, we see that the EnKF with a combined inflation scheme had no problems capturing the second pulse.

From the pressure distribution predicted by CFD, we see that whereas the first pulse created a new LEV that was shed into the wake, the second pulse occurred after the old LEV had been shed from the plate. In this particular case, the second pulse was initiated just as a new, replacement LEV was developing. We see from Fig. 32, both in the CFD vorticity contours (top right) and in the vortex blob distribution predicted by the EnKF with combined inflation (top left), that any new vortex structure created by the second pulse was merged into the newly developing LEV.

At 3.5 convective times, the second pulse has not been applied yet, so we expect the same distributions of vorticity between the single pulse case and the two pulses case. Interestingly, if we compare the vortex blob distributions in Fig. 30 and those listed in Fig. 21, we see that the distributions predicted with multiplicative covariance inflation look very different across the two cases. In contrast, the vortex blob distributions predicted by the combined inflation scheme agree well. This reinforces the idea that without careful tuning of the additive inflation or some means of localizing the Kalman gain matrix,¹² the EnKF and the nonlinear system dynamics can work together to amplify spurious correlations and prevent the ensemble from actually converging.

IV. Conclusions

In this work, we have developed a dynamic estimation framework for two-dimensional disturbed separated flows, in which surface pressure measurements are used to augment a discrete vortex model, to collectively predict the full state of the flow. The vortex model utilizes advecting vortex blobs released from the leading and trailing edges of a flat plate. At the leading edge, the strength of shed vorticity is determined by the critical leading-edge suction parameter (LESP). The estimation framework uses an ensemble Kalman filter (EnKF), in which a collection of randomly-initialized vortex models are used to predict the state of the flow, continuously updated with the sampled surface pressures from the truth case. The estimation framework was demonstrated on impulsive motion of a flat plate at 20 degrees fixed angle of attack, at which the flow is inherently separated. The vortex-based estimator performs well to estimate both the baseline flow as well as the disturbance of the flow by incident gusts.

The state vector in our implementation of the EnKF consists of the vortex positions and strengths as well as the critical LESP. It is important to stress that we have no dynamical model for the critical LESP; rather, we rely only on the measured surface pressures along the plate to estimate this parameter via the Kalman gain. In so doing, we have implicitly shown that the critical LESP—that is, the tolerance of the flow to relative motion of the fluid about the edge—changes dynamically in response to a gust, and thus, triggers the appropriate release (and, at times, suppression) of new vorticity at the leading edge in such an aerodynamic disturbance. We are currently investigating further whether other forms of disturbance, such as surface actuator pulses or rigid-body excursions, can be similarly represented and observed in the critical LESP.

In our demonstration of the estimation framework in this paper, we have relied on truth measurements from a high-fidelity numerical simulation of the flow past a flat plate. However, the method should be agnostic to the source of pressure measurements, especially as it is intended to be used for real-time flow control. And ultimately, we would like to replace these numerically computed pressure measurements with experimental data. In ongoing work, we are exploring the number and location of pressure sensors that ensure a good estimate.

V. Acknowledgments

Support by the U.S. Air Force Office of Scientific Research (FA9550-14-1-0328) with program manager Dr. Douglas Smith is gratefully acknowledged.

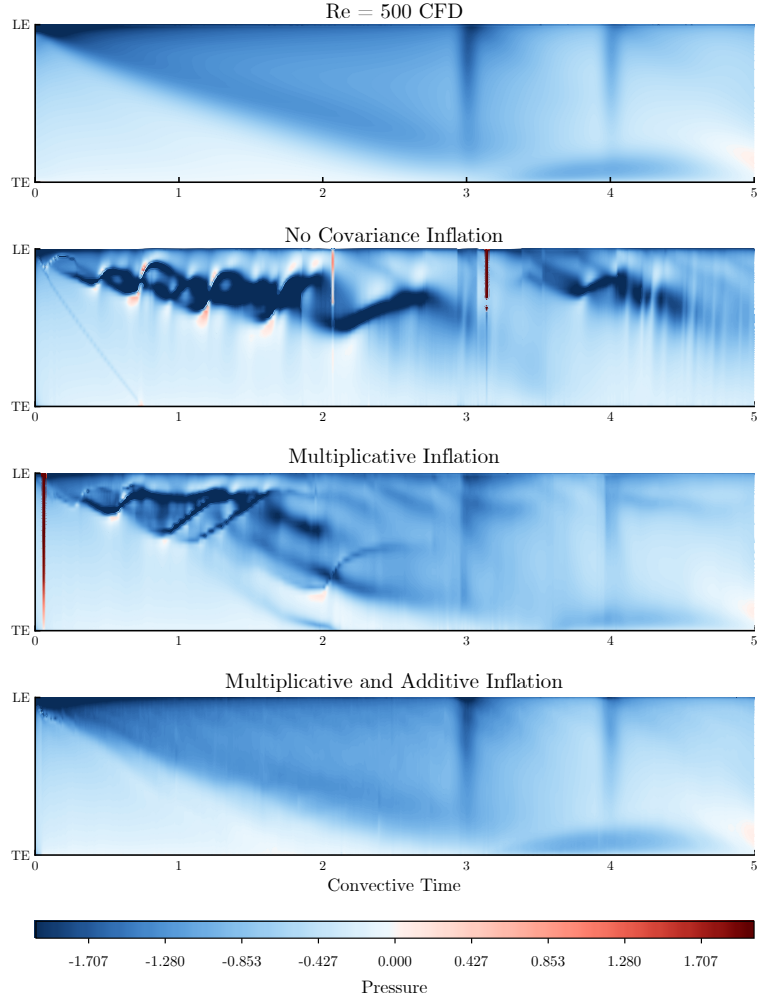


Figure 24. Comparison of the pressure coefficient distribution along the plate over time between the CFD results and EnKF predictions with various covariance inflation settings for the two pulses case

References

- ¹X. An, D. R. Williams, J. D. Eldredge, and T. Colonius. Modeling dynamic lift response to actuation. 54th AIAA Aerospace Sciences Meeting, San Diego, CA. AIAA Paper 2016-0058, 2016.
- ²Jeffrey L. Anderson and Stephen L. Anderson. A Monte Carlo Implementation of the Nonlinear Filtering Problem to Produce Ensemble Assimilations and Forecasts. *Monthly Weather Review*, 127(12):2741–2758, 1999.
- ³Salman A. Ansari, Rafal Zbikowski, and Kevin Knowles. Non-linear unsteady aerodynamic model for insect-like flapping wings in the hover. Part 2: implementation and validation. *Proc. Inst. Mech. Eng. Part G J. Aerosp. Eng.*, 220:169–186, 2006.
- ⁴C. E. Brown and W. H. Michael. Effect of Leading-Edge Separation on the Lift of a Delta Wing. *J. Aeronaut. Sci.*, 21(10):690–694, 1954.
- ⁵Gerrit Burgers, Peter Jan van Leeuwen, and Geir Evensen. Analysis Scheme in the Ensemble Kalman Filter. *Monthly Weather Review*, 126(6):1719–1724, 1998.
- ⁶D. Darakananda, J. D. Eldredge, T. Colonius, and D. R. Williams. A vortex sheet/point vortex dynamical model for unsteady separated flows. 54th AIAA Aerospace Sciences Meeting, San Diego, CA. AIAA Paper 2016-2072, 2016.
- ⁷Andre Fernando de Castro da Silva and Tim Colonius. An EnKF-based Flow State Estimator for Aerodynamic Flows. 8th AIAA Theor. Fluid Mech. Conf., AIAA Paper 2017-3483, 2017.
- ⁸J. D. Eldredge and D. Darakananda. Reduced-order two- and three-dimensional vortex modeling of unsteady separated flows. 53rd AIAA Aerospace Sciences Meeting, Kissimmee, FL. AIAA Paper 2015-1749, 2015.
- ⁹Geir Evensen. Sequential data assimilation with a nonlinear quasi-geostrophic model using Monte Carlo methods to forecast error statistics. 99(C5):10143, 1994.
- ¹⁰Arthur Gelb. *Applied Optimal Estimation*. MIT press, 1974.
- ¹¹Maziar S. Hemati, Jeff D. Eldredge, and Jason L. Speyer. Improving vortex models via optimal control theory. *J. Fluids Struct.*, 49:91–111, 2014.

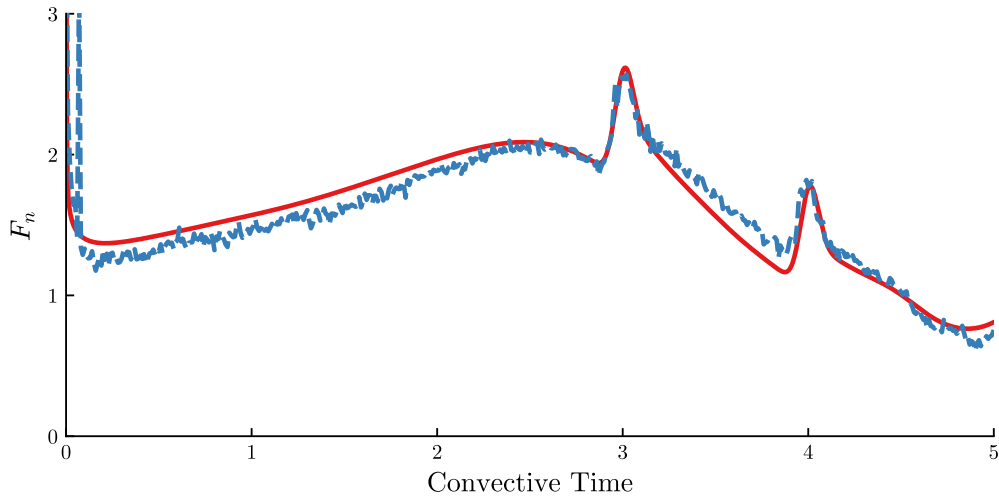


Figure 25. Comparison of the predicted normal force between (—) CFD results, and (—) EnKF ensemble mean for the two pulses case.

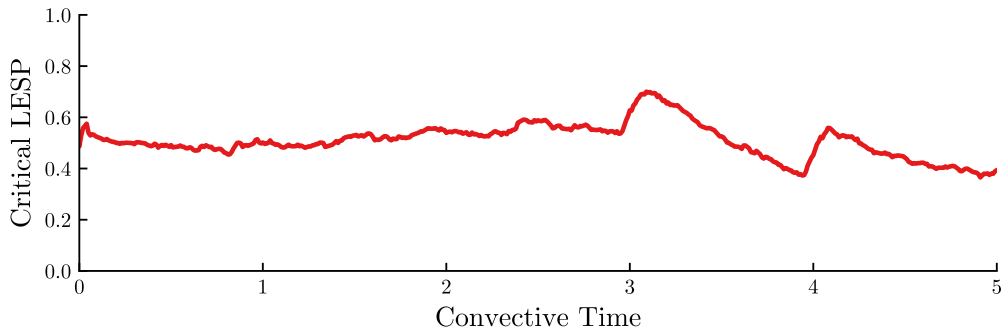


Figure 26. Time history of the ensemble mean value of the critical LESP for the two pulses case

¹²P. L. Houtekamer, Herschel L. Mitchell, P. L. Houtekamer, and Herschel L. Mitchell. A Sequential Ensemble Kalman Filter for Atmospheric Data Assimilation. *Monthly Weather Review*, 129(1):123–137, 2001.

¹³Joseph Katz. A discrete vortex method for the non-steady separated flow over an airfoil. *J. Fluid Mech.*, 102:315–328, 1981.

¹⁴Kiran Ramesh and Ashok Gopalarathnam. Theoretical Modeling of Leading Edge Vortices Using the Leading Edge Suction Parameter. *AIAA Appl. Aerodyn. Conf.*, pages 1–16, 6 2012.

¹⁵Kiran Ramesh, Ashok Gopalarathnam, Kenneth Granlund, Michael V. Ol, and Jack R. Edwards. Discrete-vortex method with novel shedding criterion for unsteady aerofoil flows with intermittent leading-edge vortex shedding. *Journal of Fluid Mechanics*, 751:500–538, 2014.

¹⁶Kunihiko Taira and Tim Colonius. The immersed boundary method: A projection approach. *Journal of Computational Physics*, 225(2):2118–2137, aug 2007.

¹⁷Peter Jan van Leeuwen. Comment on “Data Assimilation Using an Ensemble Kalman Filter Technique”. *Monthly Weather Review*, 127(6):1374–1377, 2010.

¹⁸Chengjie Wang and Jeff D. Eldredge. Low-order phenomenological modeling of leading-edge vortex formation. *Theor. Comput. Fluid Dyn.*, 8 2012.

¹⁹Jeffrey S. Whitaker and Thomas M. Hamill. Evaluating Methods to Account for System Errors in Ensemble Data Assimilation. *Monthly Weather Review*, 140(9):3078–3089, 2012.

²⁰X. Xia and K. Mohseni. Lift evaluation of a two-dimensional pitching flat plate. *Physics of Fluids*, 25(9), 2013.

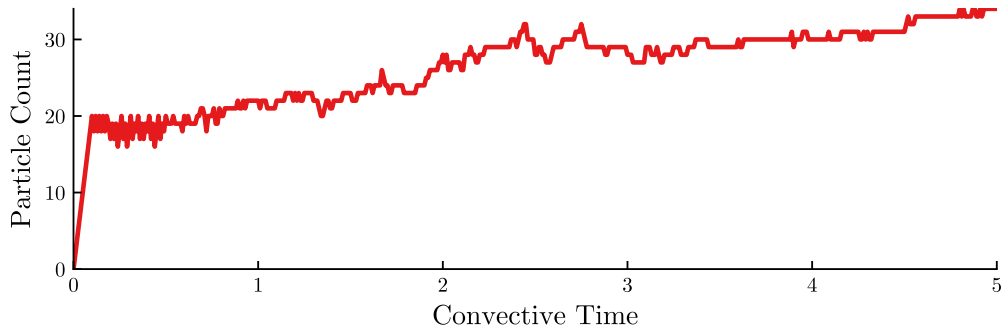


Figure 27. Number of vortex blobs used in the model over time when a combined multiplicative and additive covariance inflation is used for the two pulses case

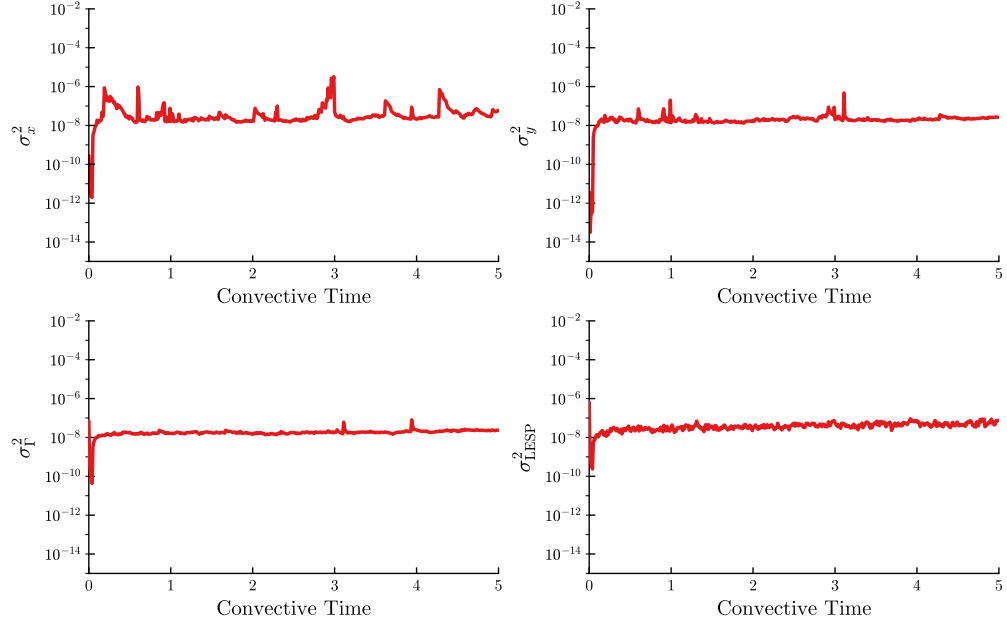


Figure 28. Ensemble variances for the two pulses case with both multiplicative and additive covariance inflation

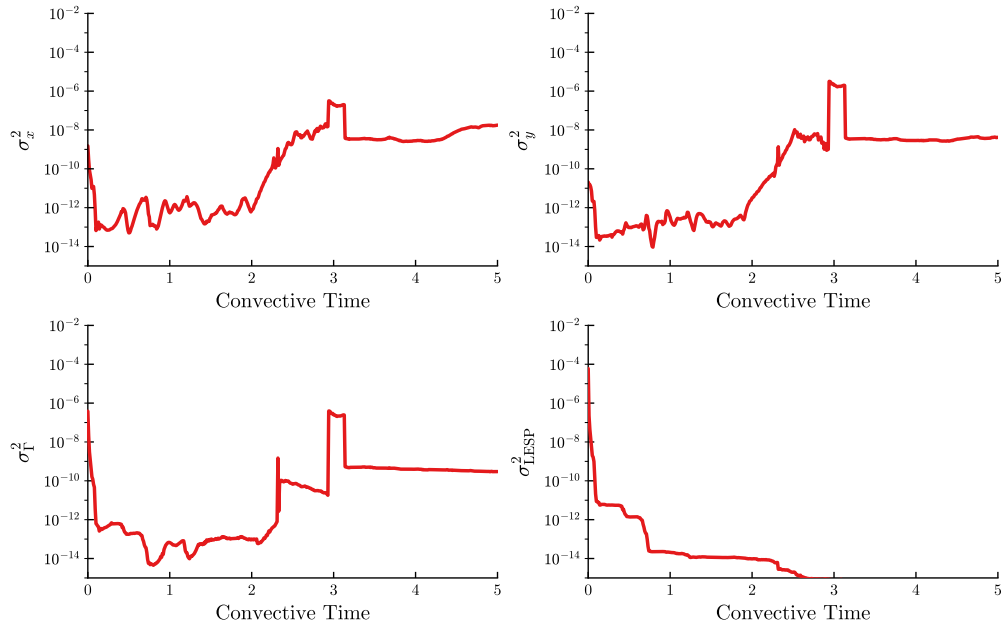


Figure 29. Ensemble variances for the two pulses case without covariance inflation

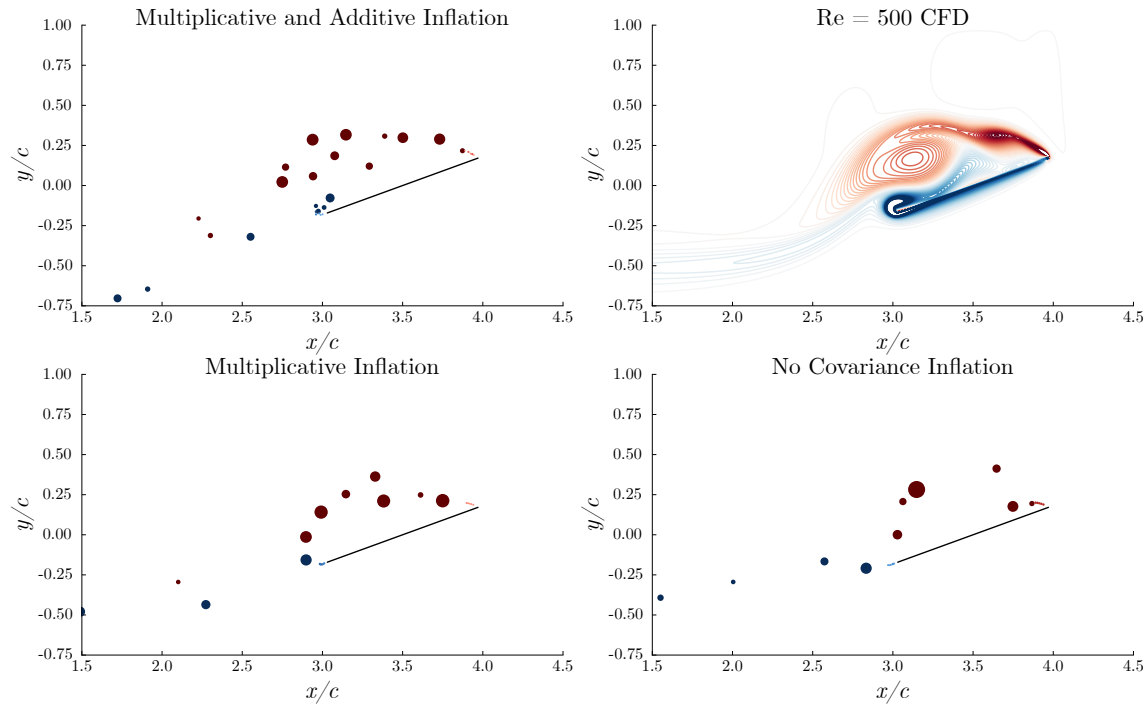


Figure 30. Comparison of the vorticity distribution for the two pulses case at 3.5 convective times.

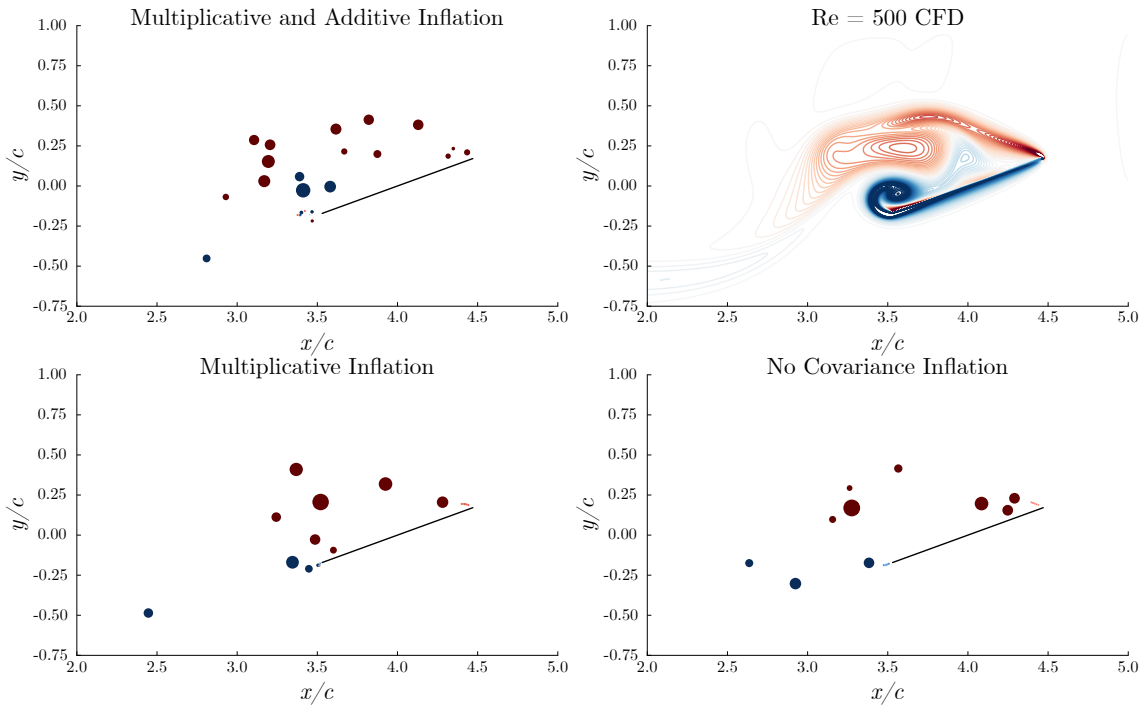


Figure 31. Comparison of the vorticity distribution for the two pulses case at 4 convective times.

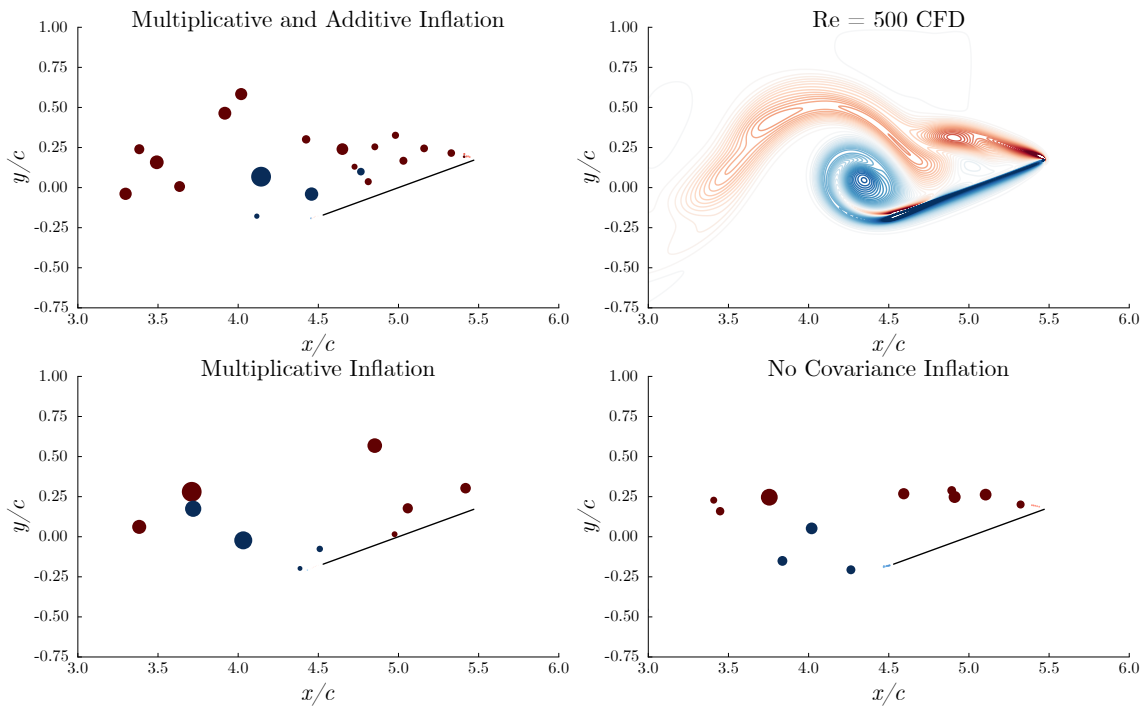


Figure 32. Comparison of the vorticity distribution for the two pulses case at 5 convective times.